REVIEW

Check for updates

Advances in functional guest materials for resistive gas sensors

Ze Wang, [ID] [a] Lei Zhu, [ab] Jingzhao Wang, [a] Rui Zhuang, [c] Pengfei Mu, [c] Jianan Wang [ID] *[a] and Wei Yan [ID] [a]

Resistive gas sensors are considered promising candidates for gas detection, benefiting from their small size, ease of fabrication and operation convenience. The development history, performance index, device type and common host materials (metal oxide semiconductors, conductive polymers, carbon-based materials and transition metal dichalcogenides) of resistive gas sensors are firstly reviewed. This review systematically summarizes the functions, functional mechanisms, features and applications of seven kinds of guest materials (noble metals, metal heteroatoms, metal oxides, metal–organic frameworks, transition metal dichalcogenides, polymers, and multiple guest materials) used for the modification and optimization of the host materials. The introduction of guest materials enables synergistic effects and complementary advantages, introduces catalytic sites, constructs heterojunctions, promotes charge transfer, improves carrier transport, or introduces protective/sieving/enrichment layers, thereby effectively improving the sensitivity, selectivity and stability of the gas sensors. The perspectives and challenges regarding the host–guest hybrid materials-based gas sensors are also discussed.

1. Introduction

There are various types of gases existing in the human environment that affect the environmental quality and human

[a]Department of Environmental Science and Engineering, Xi'an Key Laboratory of Solid Waste Recycling and Resource Recovery, State Key Laboratory of Multiphase Flow in Power Engineering, School of Energy and Power Engineering, Xi'an Jiaotong University, 28 Xianning West Road, Xi'an 710049, China. E-mail: wangjn116@xjtu.edu.cn

[b]School of Physics and Electrical Engineering, Weinan Normal University, Chaoyang Street, Weinan, 714099, China

[c]Chambroad Chemical Industry Institute Co.,Ltd, Boxing Economic Development Zone, 256500, Shandong Province, China

safety, such as toxic, flammable, explosive, and indicator gases.[1–3] High-performance gas detecting devices are needed to monitor environmental pollution, realize the early warnings about the dangerous gases, assist in the early diagnosis of disease, and aid in food industry production.[4–7] Gas sensor technology is one of the most promising candidates for gas detection and has become a hotspot in monitoring the environment, safety, and health in recent years, benefiting from the advantages of their small size, ease of fabrication, low power consumption and easy operation.[8–11]

To date, many types of gas sensors with different working mechanisms have been developed, *e.g.*, catalytic combustion gas sensors,[12] electrochemical gas sensors,[13] infrared

Ze Wang is an M.A. student in the Department of Environmental Science and Engineering at Xi'an Jiaotong University. His current research interests focus on the design of functional nanomaterials and the application of gas sensing technology in the detection of battery thermal runaway and environmental pollutants.

Lei Zhu obtained her PhD degree at the School of Energy and Power Engineering at Xi'an Jiaotong University. Currently, she is a lecturer at the School of Physics and Electrical Engineering at Weinan Normal University. Her research interests focus on the preparation and design of one-dimensional metal oxides as well as the application of high-sensitivity gas sensors in the field of environmental pollution monitoring.

absorption gas sensors[14] and resistive gas sensors.[15–17] Among them, the resistive gas sensor exhibits attractive advantages, including higher sensitivity, faster response/recovery times, greater stability/repeatability, ease of operation and integration into portable devices.[18–20] Based on these advantages, the resistive gas sensor has been widely studied and occupies a large market share.[21] At present, resistive gas sensors with various types of metal oxide semiconductors (MOSs, *e.g.*, SnO_2,[22] ZnO (ref. 8) and In_2O_3 (ref. 4)) as the host sensing component have been commercialized, and sensing materials like conductive polymers (CPs) and carbon-based materials have also been widely studied.[23–25] However, just adopting single-component materials still faces some severe challenges. For example, MOSs suffer from high operating temperatures and poor selectivity; CPs suffer from poor stability and low sensitivity; carbon-based materials have the problems of poor reversibility.[9,26] To date, numerous previously reported studies have used optimization methods like morphology modulation,[27] UV irradiation,[28] and low-temperature plasma treatment[29] for better gas-sensing performance. Although these methods can improve the sensitivity of the material to a limited extent, it is difficult to change the characteristic defects of the materials themselves and the available sensing performance still cannot meet the requirements of practical application. A reliable solution for these drawbacks is the introduction and utilization of functional guest materials.

Guest materials are functional components that can optimize the gas sensing properties of the host materials. There are many ways for different types of guest materials to functionalize and optimize host materials. For example, noble metals can introduce catalytic sites and contribute to fast response, high sensitivity and low operating temperature *via* chemical/electronic sensitization.[30] Metal oxides can construct heterojunctions with semiconductor host materials, thus changing the interface potential energy barriers as well as regulating the transfer of electrons and holes.[31] Functional membranes (metal–organic frameworks (MOFs) and polymers) can act as protective/sieving/enrichment layers, thereby effectively
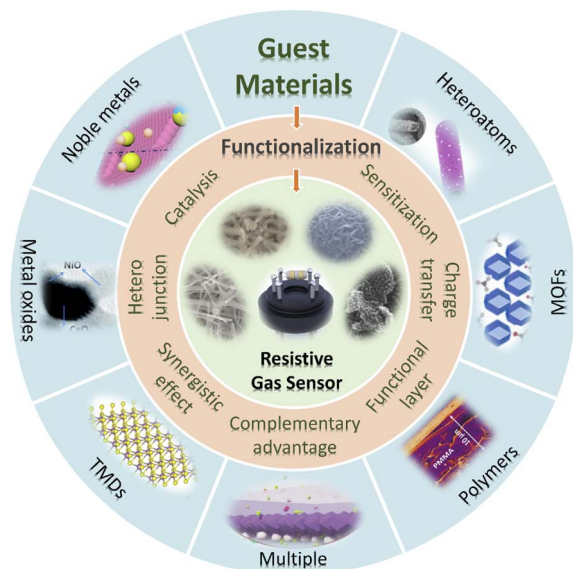

Fig. 1 Functional guest materials for resistive gas sensors discussed in this review.

improving the stability/selectivity/sensitivity of the sensor.[26,32–34] In addition, the hybridization of host–guest materials is usually accompanied by synergistic effects and complementary advantages.[30] Therefore, the introduction of guest materials is an effective way to improve the sensing performance and overcome the defects of the host materials.

This article firstly concentrates on the development and configuration types of resistive gas sensors, and the gas sensing mechanism and the advantages/disadvantages of various host materials are briefly introduced. Furthermore, this article presents a comprehensive review of the recent research efforts and developments on various functional guest materials used in resistive gas sensors, referring to the enhancement mechanism of gas sensing performance, preparation and design of host–guest hybrid materials and their application in resistive gas sensors (Fig. 1).

Jianan Wang is currently an associate professor in the Department of Environmental Science and Engineering at Xi'an Jiaotong University. He received his PhD degree from the School of Energy and Power Engineering at Xi'an Jiaotong University. His research interests include Li-ion/Li–S/Li-metal batteries, solid-state batteries, advanced energy storage technologies (including the development of high-performance commercial battery materials, battery integration and thermal management), and gas sensor technologies for environmental monitoring.

Wei Yan is currently a professor in the Department of Environmental Science and Engineering at Xi'an Jiaotong University and the leader of Xi'an Key Laboratory of Solid Waste Recycling and Resource Recovery. He received his PhD degree from the Institute of Polymer Science at Nankai University in 1997. His research interests include energy and environmental materials, water treatment and resource utilization, advanced oxidation technology, lithium battery materials and recycling technology, etc.

2. Introduction to resistive gas sensors

A resistive gas sensor is a device that can effectively transform the gas changes in the surrounding environment into resistance signals. When the sensing material reacts with or adsorbs the gas molecules, the electrons or holes will be generated and transferred in the material, and further change the resistance of the sensing material. To develop high-performance resistive gas sensors, before selecting guest materials for functionalization, it is necessary to choose appropriate substrate devices and host materials as well as to deeply understand the sensing mechanisms of various host materials. Herein, the development history, performance indexes, devices and host materials for resistive gas sensors are introduced.

2.1. Development history of resistive gas sensors

In the early 1950s, Brattain and Bardeen[35] demonstrated for the first time that some semiconductor materials (such as Ge) could change their electrical resistance depending on their exposed environment, which laid the foundation for the birth of resistive gas sensors. In 1962, Seiyama et al.[36] reported the first resistive gas sensing device that adopted the ZnO film as the sensing layer and could operate at 485 °C. In 1967, following Seyama's work, Shaver[37] further demonstrated that modifying the MOSs with the appropriate noble metals (Pt, Pd, Rh, etc.) could significantly improve their inherent gas-sensing properties, benefiting from their excellent catalytic properties. Since then, various guest materials used in resistive gas sensors have been continuously explored to greatly enhance the sensing performance of resistive gas sensors.

In 1971, Taguchi patented the first resistive gas sensor with tin dioxide (SnO_2) serving as the sensing material for practical applications. The primary application of these commercialized devices was only employed as alarms to prevent accidents and fires by monitoring the presence of hazardous levels of explosive gases.[21] In the 1980s, the field of resistive gas sensors experienced a significant expansion, becoming one of the most active research areas in the sensor community. In 1983, Nylander et al.[38] firstly reported an ammonia sensor based on the conductive polymer (polypyrrole (PPy)) as the sensing material. Since then, a series of CPs such as PPy, polythiophene (PTh) and polyaniline (PANI), have been widely used as sensing materials in resistive gas sensors. With the increasingly developed nanotechnologies and the emergence of various carbon-based materials, carbon nanotubes and graphene have also been gradually applied in resistive gas sensors.[39,40] In addition to MOSs, CPs and carbon-based materials, other host sensing materials with high sensing responses have also been developed recently, such as nitrides (g-C_3N_4,[41] h-BN,[42] etc.), transition metal dichalcogenides (TMDs, such as MoS_2,[43] $MoSe_2$,[44] WS_2,[45] etc.), ferrites ($ZnFe_2O_4$,[46] $CuFe_2O_4$,[47] $LaFeO_3$ (ref. 19) etc.), black phosphorous,[48] MXenes[49] and organic frameworks.[50]

2.2. Performance index for the resistive gas sensors

The four most critical indexes for evaluating sensor performance are defined as '4S', i.e. sensitivity, speed (response/recovery times), selectivity and stability. Sensitivity reflects the change rate of sensor resistance in a certain concentration of the target gas. It is defined as R_a/R_g for n-type semiconductors and R_g/R_a for p-type semiconductors. R_a is the resistance of the gas sensor in air, and R_g is the resistance of the gas sensor in the gas to be measured.[18] A higher response means a higher sensitivity of the gas sensor to the gas to be measured. Response/recovery time is a parameter that reflects the response speed of the gas sensor to detect the target gas. The time it takes for the sensor to achieve 90% of the total resistance change during adsorption and desorption is defined as response time and recovery time, respectively. Selectivity refers to the sensor's ability to identify the measured gas and to suppress the interference gas, also known as cross sensitivity. In mixed gas detection, the selectivity is very important; poor selectivity will affect the qualitative identification of the gas to be measured, and further limit the quantitative analysis; stability represents the long-term reliability and service life of the gas sensor, aiming at evaluating the resistance of the sensor to various influencing factors other than gas concentration.

In addition to the above 4 basic indexes, the operating temperature, repeatability, lower limit of detection, and linearity are also essential parameters for measuring its sensing performance. An ideal gas sensor has low operating temperature, high sensitivity, short response/recovery times, outstanding selectivity and excellent stability.[51,52] It is almost impossible to combine all properties for a single material. Only by introducing functional guest materials, overcoming the defects of single materials and improving the performance indexes of the sensor can the resistive gas sensor be better commercialized and applied. Therefore, the study of guest material is of great significance.

2.3. Devices of resistive gas sensors

The type of resistive gas sensor device is also an important factor that affects the gas sensing performance. Different resistive gas sensor devices always have different characteristics, and their suitable sensing materials and application scenarios are also different. The common resistive gas sensor devices can be divided into the following four categories: tubular gas sensors, interdigitated electrode (IDE)-based gas sensors, flexible/wearable gas sensors and Micro-Electro-Mechanical System (MEMS)-based gas sensors.[53–58]

As shown in Fig. 2a, a tubular gas sensor consists of a ceramic tube, a Ni–Cr heater, gold signal electrodes, Pt wires, a sensing film and a base.[53] At present, the ceramic tube type is the dominant type of resistive gas sensor, mainly because of its advanced preparation technology and low cost.[59,60] The circuit diagram of the tubular gas sensor is shown in Fig. 2b. The heater placed in the ceramic tube can provide a high operating temperature. The high thermal resistance of the ceramic allows the gas sensor to work at a higher temperature. However, the tubular gas sensors always suffer from a limited electrode area to load the sensing materials, which makes its available sensing response not high enough. Therefore, tubular sensors are more suitable for sensing materials simultaneously with high sensitivity, high operating temperature and good thermal stability.
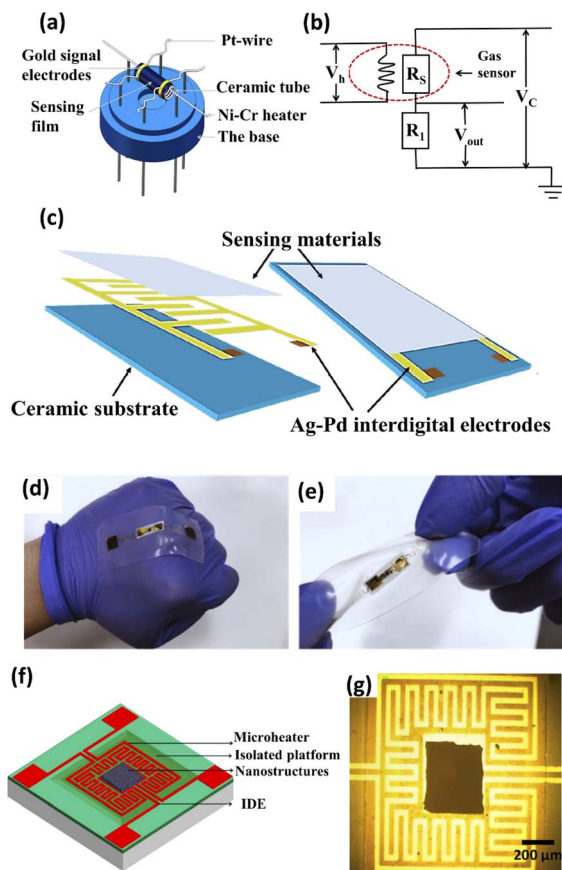
Fig. 2 (a) Schematic illustration of the structure of a tubular gas sensor. (b) Circuit diagram of a tubular gas sensor. This figure has been reproduced with permission from ref. 53, Elsevier, Copyright 2020. (c) Schematic illustration of the structure of an IDE gas sensor. This figure has been reproduced with permission from ref. 54, Elsevier, Copyright 2020. Demonstration of the flexible gas sensor deformed by (d) making a fist, (e) twisting. This figure has been reproduced with permission from ref. 55, Elsevier, Copyright 2020. (f) Schematic diagram and (g) photographic image of a MEMS–based gas sensor. This figure has been reproduced with permission from ref. 58, Elsevier, Copyright 2016.

The IDE-based gas sensors are characterized by their miniaturization, fast response and low-cost mass fabrication.[2,61] The IDE-based gas sensors have electrodes with periodic patterns in the finger-like or comb-like surface, which consists of a ceramic substrate, interdigital electrodes and sensing materials (Fig. 2c).[54] The structure of the IDE can significantly increase the contact area between the electrode and gas sensing materials, enabling the high sensitivity of the gas sensors even at a low temperature.

The flexible/wearable gas sensors are mainly composed of two parts: a flexible substrate and electrode (Fig. 2d and e).[55] The flexible/wearable gas sensor is one of the most popular gas sensors in recent years due to its being lightweight and portable with excellent electrical performance and high integration.[55] Its gas sensing properties will not change significantly when stretched, tilted or bent, but it exhibits low resistance under high temperature.[62] Different flexible substrates, such as polyethylene-terephthalate (PET), polyimide (PI) and Kapton, have been used

for the flexible and wearable gas sensors.[63–66] Carbon-based materials, such as graphene, graphene oxide (GO), reduced graphene oxide (rGO), single-wall carbon nanotubes (SWCNT), etc., have been reported to be ideal candidates for flexible/wearable gas sensors due to their high mechanical strength, good stability, high carrier mobility and good flexibility.[23,67]

MEMS is an electromechanical system with three-dimensional (3D) geometry (Fig. 2f and g).[58] It is constructed on a silicon-wafer platform based on photolithography microelectronics manufacturing and post-processing techniques.[66] These processes allow designers to accumulate different sensor arrays on a sensor platform to meet the requirements of integration, intelligence and multifunction. Nanoscale MOS materials combined with MEMS technology are widely used in the field of gas sensors due to their greatly reduced size, low cost and low power consumption.[68] Typically, compared with a conventional tubular gas sensor equipped with a heater consuming about 1–5 W during its operation, MEMS-based gas sensors consuming less than 30–50 mW can reach a working temperature of up to 500 °C.[69]

2.4. Host materials and sensing mechanisms

The sensing mechanism of a host–guest hybrid material is generally governed by the host material.[26] For the same kind of guest material, the gas-sensing enhancement mechanisms and the host–guest interactions may be different when it is hybridized with different host materials. Therefore, it is necessary to understand the material type, advantages/disadvantages and the sensing mechanisms of the host materials before studying the guest materials, so as to select appropriate guest materials for functionalization according to the characteristics of the host materials. Herein, we mainly introduce four types of host materials: MOSs, CPs, carbon-based materials and TMDs.

The gas-sensing mechanism of the MOS-based resistive gas sensor is highly dependent on the surface reactions between target gas molecules and chemisorbed oxygen species (O^{2-}, O^-, and O_2^-).[70] At an elevated temperature, oxygen molecules in air are chemisorbed on the surfaces of metal oxides by trapping electrons in MOSs, generating either electron depletion regions in the case of n-type MOSs or hole accumulation layers for p-type MOSs. Reducing or oxidizing gas molecules will react with the chemisorbed oxygen and are adsorbed on MOSs, modulating the thickness of the electron depletion layers or hole accumulation layers, resulting in a resistance change of the gas sensors.[26]

MOSs applied in resistive gas sensors are mainly divided into n-type (SnO_2,[71] ZnO,[72] TiO_2,[73] In_2O_3,[4] etc.) and p-type (CuO,[74] NiO,[75] etc.) MOSs. In general, MOSs possess wide band gaps, excellent physical/chemical properties and unique structures (small grain size and high porosity), enabling the superiorities of high sensitivity, fast response and good stability when used as gas-sensitive materials.[22] However, they also suffer from some disadvantages including high working temperature, low gas selectivity and serious baseline drift.[76] Therefore, the main purpose of the introduction of guest materials to optimize MOSs in resistive gas sensors is to reduce the operating temperature and improve the gas selectivity of MOSs.

The sensing mechanism of CPs can be divided into the following three different types according to the target gases: those that (1) change the resistance between conducting polymer chains by REDOX reactions (*e.g.* NO_2, CO, NH_3);[77] (2) adjust the distance between the molecular chains of the conductive polymer by forming hydrogen bond/dipole moment (*e.g.* H_2, NH_3), thus changing the resistance of the sensing layers;[78] (3) affect the carrier concentration in the CPs through the interaction between the adsorbed gas molecules and the charges in the conductive polymer sensitive layer, thus changing the resistance of the CPs (*e.g.* various volatile organic compounds (VOCs), H_2O).[79,80] Various CPs such as PANI, PPy and PTh have been reported for application in gas sensors due to their excellent electronic properties, low operating temperatures and intrinsic redox reactivity.[18,81] However, unsatisfactory sensitivity and poor long-term stability are two main challenges for the pure CPs as host sensing materials in resistive gas sensors, which need to be further improved by the appropriate guest modifiers.

The gas-sensing mechanism of the resistive sensors with carbon-based host materials is mainly based on their conductance changes caused by the adsorption of target analytes on their surfaces. Depending on the position of adsorption sites, the adsorbed gas molecules (1) directly interact with carbon-based materials by donating electrons or depriving electrons (intra-carbon) or (2) change the electron hopping currents among the sensing materials (inter-carbon) by the swelling effect.[26] Carbon-based materials possess large theoretical surface areas and hence can provide a large sensing area for the adsorption of gas molecules. Besides, they exhibit high carrier mobility and low resistance at room-temperature conditions but endure low response, poor selectivity and low reproducibility.[23] Therefore, the introduction of guest materials is necessary to optimize the sensing performance factors (stability, repeatability and response/recovery time) of carbon-based materials.

TMDs are an emerging class of two-dimensional (2D) inorganic compounds with a general formula MX_2 (X–M–X), where M represents a layer of transition metal element from group 4 to group 10, and X represents a chalcogen element (S, Se, and Te).[9,82] TMDs are layered graphene-like materials and their sensing mechanism is similar to the intra-carbon-sensing mechanism, mainly based on the direct interaction between target analytes and sensing materials.[20,26,83] TMDs with excellent electronic, optical, and catalytic properties can realize a room-temperature gas sensing response.[13] However, their adjacent layers are connected by weak intermolecular forces, leading to the special aggregation and self-stacking effects, hence reducing the permeability and surface active sites of TMDs. Another serious problem for TMDs-based host materials is that they are easily oxidized in an air environment.

3. Functional guest materials in resistive gas sensors

As mentioned above, single gas-sensitive materials, such as MOSs, CPs, carbon-based materials and TMDs, generally have their advantages and disadvantages. It is necessary to introduce functional guest materials to improve the gas sensing properties of the sensors. Herein, seven typical guest materials (noble metals, metal heteroatoms, metal oxides, metal–organic frameworks (MOFs), TMDs, polymers, and multiple guest materials) used in resistive gas sensors are reviewed according to functions, advantages/disadvantages and mechanisms.

3.1. Noble metals

The common noble metals in resistive gas sensors mainly include Pd,[84] Pt,[85] Ag,[86] Au,[87] *etc.* When used as the guest materials, these noble metals are generally modified onto host materials to form heterostructural nanoparticles, improving the sensitivity and reducing the working temperature of gas sensors through catalytic and adsorption effects. The functional mechanisms of the noble metals as the guest materials mainly depend on electronic sensitization or chemical sensitization.[88] Under normal circumstances, the work function of the noble metals is higher than that of the MOS gas-sensitive materials, and requires equilibrium and charge redistribution. At the interface of the noble metal and MOS, the conduction band will bend to form a Schottky barrier, and the electrons in the conduction band of the MOS sensing material further are transferred to the noble metal nanoparticles to form an interface dipole layer. This process prevents the recombination of separated electron–hole pairs, thereby increasing the gas response of the MOS. This phenomenon is called electronic sensitization (Fig. 3a). Chemical sensitization refers to the adsorption and dissociation enhancement of gases on the surface of sensing materials (Fig. 3b). Noble metal nanoparticles can promote the adsorption of oxygen molecules and the formation of oxygen ions through chemical reduction, and then the oxygen ions spill over to the surface of sensing materials, thus increasing the concentration of oxygen ions. The target gas molecules can also be directly attached to the noble
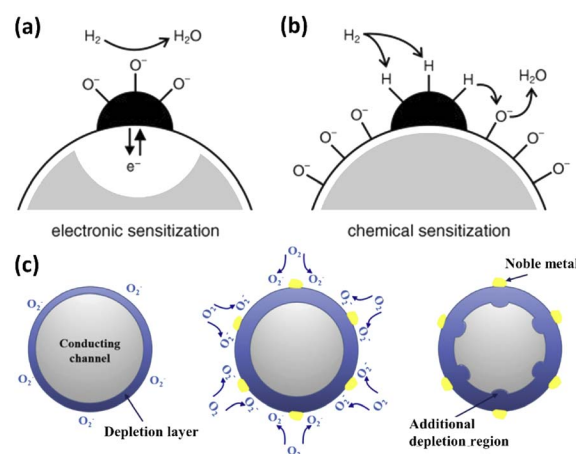

Fig. 3 Mechanisms of (a) electronic sensitization and (b) chemical sensitization of noble metals. This figure has been reproduced with permission from ref. 88, Wiley, Copyright 2005. (c) Schematic illustration of the spillover effect. This figure has been reproduced with permission from ref. 8, Elsevier, Copyright 2017.

metal nanoparticles, migrating to the surface of the host MOS and further reacting with oxygen ions. This spillover effect can significantly improve the gas sensing performance (Fig. 3c).[8]

Jaroenapibal *et al.*[89] fabricated Ag-doped WO_3 by the electrospinning method. Porous mats of nanofibers comprising monoclinic WO_3 nanoparticles (28–39 nm) incorporated with small Ag particles were observed. At 225 °C, the response sensitivity of 3 mol% Ag-doped WO_3 nanofibers to 5 ppm NO_2 gas was 90.3, more than 9 times higher than that of undoped WO_3 nanofibers. The Ag–WO_3 also showed high selectivity to NO_2 gas as compared with other interfering gases (CH_4, NH_3, SO_2 and H_2S). The enhancement of the sensing performance is mainly attributed to the catalytic effect, enhanced electron sensitization and increased oxygen vacancy content caused by Ag nanoparticles (Fig. 4a and b). Significant decreases in gas responses were observed in the samples with higher Ag dopant levels (5 and 10 mol%), where the crystallite size of Ag nanoparticles became too large and hindered their catalytic effects (Fig. 4c). Li *et al.*[90] synthesized pure and Au-loaded Co_3O_4 porous hollow nanocages using ZIF-67 as a sacrificial template. Due to the spillover effect of Au, the content of adsorbed oxygen was increased from 9.1% of pure Co_3O_4 to 27.5% of Au/Co_3O_4, enhancing the catalytic activities for acetone adsorption and the reactions were also enhanced. The response of Au/Co_3O_4 to 100 ppm acetone at 190 °C was 14.5, and the limit of detection was 1 ppm. Meanwhile, the addition of Au significantly changed

the original morphology of Co_3O_4 and formed coarser surfaces and openings, which improved the transport of gas molecules through Au/Co_3O_4. This improved gas accessibility could also account for the significantly increased recovery speed of Au/Co_3O_4 (280 s) as compared to pure Co_3O_4 (7559 s).

The introduction of Pd can greatly improve the sensitivity and selectivity of the H_2 sensor.[91] Pd is widely used as the gas sensing material for H_2 because of its superior capacity to absorb and catalyze H_2.[26,92] Wang *et al.*[93] prepared 2D porous TiO_2 nanosheets by a graphene oxide template method and further introduced Pd nanoparticles onto these nanosheets by an impregnation technique to obtain the final Pd–TiO_2 nanosheets. The H_2 sensor based on Pd–TiO_2 nanosheets exhibited an instantaneous response, low detection limit (1 ppm), good selectivity and linear response (Fig. 4d–f), which were mainly attributed to the synergistic effect between Pd and TiO_2 (including the high adsorption ability of Pd–TiO_2 toward both O_2 and H_2 as well as the effective catalysis ability of Pd toward H_2) and the unique porous 2D structure (Fig. 4g).

Noble metals-decorated carbon-based materials-based gas sensors can reveal the effective gas sensing capability at low temperature.[94] This is mainly due to the synergy of the catalytic effect of noble metals and the prompt electron transfer of carbon-based materials between the target gas and metal electrodes.[95] Kwon *et al.*[85] prepared high-performance toluene (C_7H_8) gas sensor by using the Pt-multiwalled carbon nanotubes
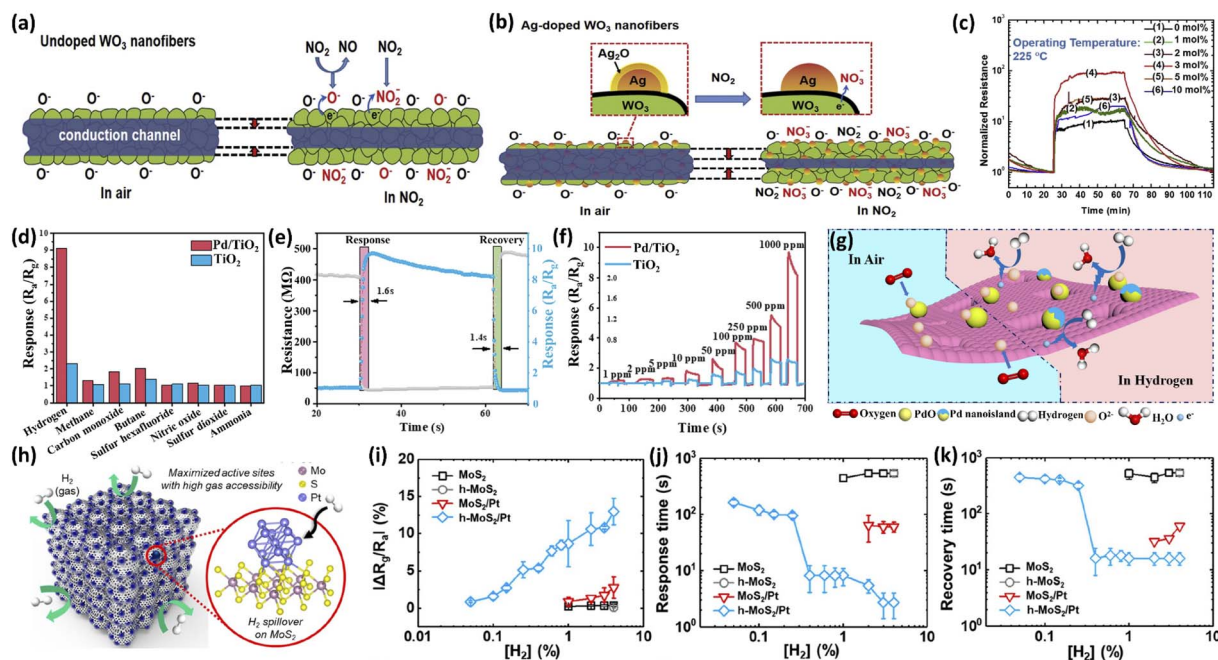

Fig. 4 Schematic diagram of the NO_2 sensing mechanism of (a) WO_3 and (b) Ag-loaded WO_3 nanofibers. (c) Resistance plots of the WO_3 and Ag-loaded WO_3 nanofibers measured in air and 5 ppm NO_2 at operating temperatures of 225 °C. This figure has been reproduced with permission from ref. 89, Elsevier, Copyright 2018. (d) Selectivity of the TiO_2 and Pd/TiO_2 toward different reference gases (1000 ppm) at 230 °C. (e) Response/recovery curve of the sensor based on Pd/TiO_2 toward 1000 ppm H_2 at 230 °C. (f) Dynamic response curves of the sensors based on TiO_2 and Pd/TiO_2 toward 1 ppm to 1000 ppm H_2 at 230 °C. (g) Schematic illustration of the H_2 gas-sensing mechanism of Pd/TiO_2. This figure has been reproduced with permission from ref. 93, Elsevier, Copyright 2021. (h) Schematic illustration of the structure and sensing mechanisms of h-MoS_2/Pt. (i) Response, (j) response time, and (k) recovery time of sensors based on MoS_2, h-MoS_2, MoS_2/Pt, and h-MoS_2/Pt. This figure has been reproduced with permission from ref. 97, American Chemical Society, Copyright 2020.

(MWCNTs) composite materials. The size of the Pt nano-particles can be optimized by controlling the predeposited Pt thickness, thus obtaining the highest sensing performance. The Pt-functionalization drastically enhanced the sensing behavior of the Pt-MWCNTs composite sensor. The response of this sensor at 150 °C could reach 3.91 to 1 ppm C_7H_8 gas (237.1% higher than pure MWCNTs) and the response/recovery times (55/70 s) were decreased by 89.2% and 92.7%, respectively. This Pt-MWCNTs sensor also showed high selectivity for C_7H_8 in comparison with other gases, including C_2H_5OH, CO, H_2, and C_6H_6. Johnson et al.[96] decorated Pd nanoparticles on graphene nanoribbon porous film for H_2 detection. Gas measurement indicated that the catalytic noble metal plays an important role in H_2 sensing and showed fast recovery/response times (6/23 s) to 40 ppm H_2 at room temperature (RT).

Noble metals loaded on TMDs can also achieve room temperature gas sensing. Park et al.[97] coated MoS_2 nanofilms on polystyrene particles by a one-step Pickering emulsification method and then loaded Pt nanoparticles on MoS_2 films. By further pyrolyzing this compound, the highly porous hollow hybrid materials (h-MoS_2/Pt) were formed. The obtained h-MoS_2/Pt possessed a high specific surface area to guarantee abundant permeable paths for H_2 molecules and maximized the active site of MoS_2 (Fig. 4h). Besides, the spillover effect of Pt nanoparticles also significantly improved the gas-sensitive performance of the original h-MoS_2. As a result, h-MoS_2/Pt achieved fast response/recovery times (8.1/16 s) and high sensitivity to H_2 at RT (Fig. 4i–k). Zhang et al.[98] demonstrated a high-performance CO sensor based on Pd-decorated WSe_2 (Pd–WSe_2) hexagonal nanosheet nanostructures. The Pd–WSe_2 thin film sensor had excellent sensing performance for CO gas, including high sensitivity (the response to 5 ppm CO at RT was 9.25), excellent repeatability, good selectivity and fast response/recovery speeds (52/97 s).

In summary, precious metals can significantly enhance the sensing performance, including sensitivity, response recovery speed, and operating temperature. However, the addition of noble metals will increase the cost, and the catalyst poisoning will cause the failure of gas sensor components. Therefore, noble metals as guest sensing materials still have certain limitations in practical application.

3.2. Metal heteroatoms

In resistive gas sensors, metal heteroatoms as the sensing guest materials are generally doped into MOSs in the form of functional ions (such as Ni^{2+}, Zn^{2+}, Al^{3+}, Ca^{2+} and Co^{3+}).[22,99–102] The doping of metal heteroatoms is widely considered a simple and effective way to elevate the performance of gas sensors. The introduction of these metal heteroatoms will change the grain size, porosity and specific surface area of the host MOSs, in turn modifying the adsorption sites and diffusion paths of the gas molecules.[103] Most importantly, it can change the energy band structure of the material. When the grain size is less than twice the Debye length, the electron depletion layer will occupy the entire grain, thereby improving the gas sensing properties of the host MOS.[17] A higher specific surface area and larger

porosity provide more adsorption sites and abundant transport channels to promote gas diffusion and improve the sensing sensitivity of the host MOS. To verify the influence of heteroatomic doping on the material energy band structure, Chen et al.[104] prepared Al-doped In_2O_3, and the changes in the In_2O_3 band gap and Fermi level caused by the addition of Al atoms were revealed by DFT calculations (Fig. 5a and b). The calculated band gap increased from 0.94 eV to 0.99 eV upon the addition of Al atoms, and the Fermi level increased from 5.17 eV to 5.24 eV. Due to the elevated Fermi level, Al-doped In_2O_3 exhibited a higher response. However, not all metal heteroatoms can improve the sensing performance of gas sensors. As shown in Fig. 5c, Chen et al.[104] also studied the doping of In_2O_3 with other metal heteroatoms and found that some dopants (such as Al, Ga and Zr) raised the Fermi level of In_2O_3, while the others (such as Ti, V, Cr, Mo, W and Sn) reduced the Fermi level. Only the former can improve the response of gas sensors.

Zhao et al.[105] synthesized Ca-doped In_2O_3 nanotubes via electrospinning and annealing technology. The average size of In_2O_3 grains initially decreased following an increase in Ca content from ≤3 mol% to ≥7 mol%. Ca doping also increased the oxygen vacancy concentration and was beneficial to the selective catalysis of ethanol (Fig. 6a and b). In particular, the sensor based on 3% Ca–In_2O_3 showed the best sensing performance toward ethanol, with high sensitivity, good selectivity, long-term stability and excellent reproducibility (Fig. 6c and d). Hjiri et al.[106] prepared Al-doped ZnO nanoparticles (Al–ZnO) by sol–gel technology for application in the CO gas sensor (the
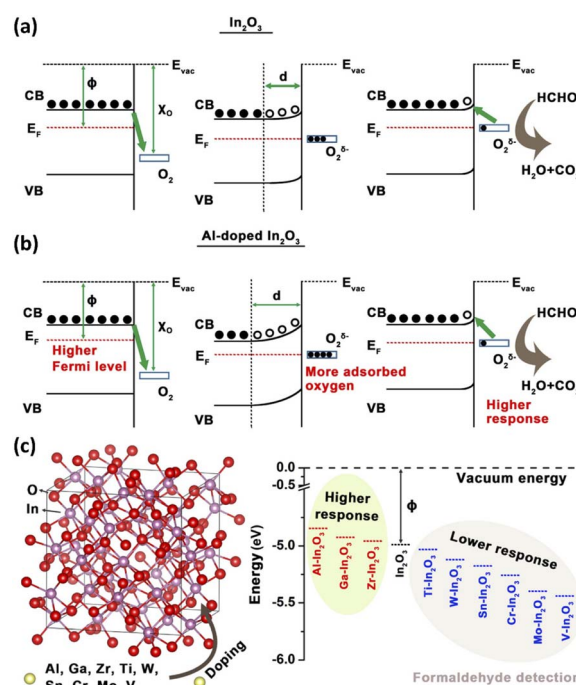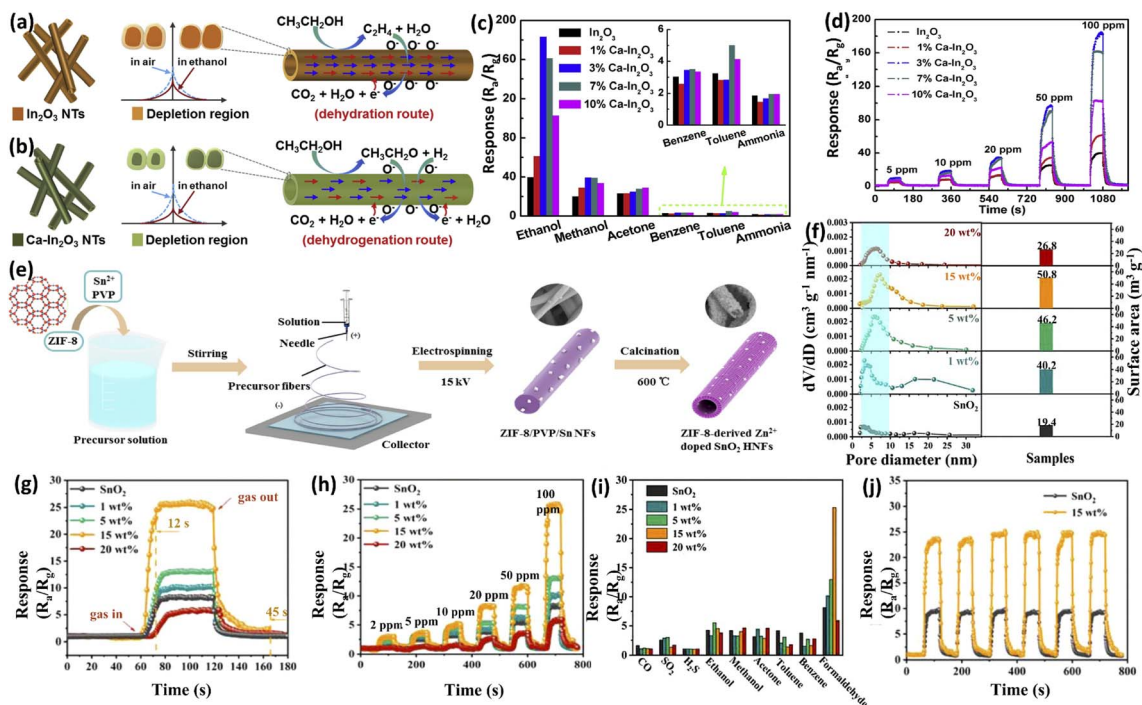

Fig. 5 Schematic energy diagram of (a) In_2O_3- and (b) Al-doped In_2O_3; (c) lattice model of 9 kinds of metal atoms doped In_2O_3 and the comparison of the Fermi energy levels of In_2O_3 materials before and after doping. This figure has been reproduced with permission from ref. 104, American Chemical Society, Copyright 2018.

Fig. 6 Schematic diagrams of (a) pure In_2O_3 and (b) Ca–In_2O_3 exposed to air and ethanol. (c) Selectivity of pure and Ca-doped In_2O_3 for various gases (100 ppm) at 240 °C. (d) Dynamic response curves of pure and Ca-doped In_2O_3 to 5–100 ppm ethanol at 240 °C. This figure has been reproduced with permission from ref. 105, Elsevier, Copyright 2019. (e) Schematic illustration of the synthetic procedure for ZZS HNFs. (f) Pore size distribution and surface areas of pristine SnO_2 and ZZS HNFs with different Zn doping amounts. Sensing properties of the sensors based on pristine SnO_2 and ZZS HNFs with different Zn doping amounts at 400 °C: (g) response/recovery curves to 100 ppm HCHO and (h) dynamic response curves to different concentrations of HCHO. (i) Responses of sensors to various 100 ppm gases at 400 °C. (j) Six dynamic response–recovery cycles of the sensors based on pristine SnO_2 and 15 wt% ZZS HNFs for the detection of 100 ppm HCHO. This figure has been reproduced with permission from ref. 22, Elsevier, Copyright 2019.

response to 50 ppm CO at 300 °C was 80, the response time was only 7 s, and the detection limit was 250 ppb). They found that Al could promote the adsorption and chemical inter-reaction of CO and O_2 to improve the gas-sensing response.

In addition, the doped nanoparticles are prone to agglomerate and reduce the specific surface area and the exposed active sites of sensitive materials, consequently resulting in the reduced gas sensing response of resistive gas sensors. To overcome this problem, our group[22] synthesized a series of MOF-derived Zn^{2+}-doped SnO_2 hollow nanofibers (ZZS HNFs) *via* the facile electrospinning method and annealing treatment for smart HCHO monitoring (Fig. 6e). Compared with the original SnO_2, all ZZS HNFs possessed a smaller pore size and larger specific surface area, indicating that MOFs can be used as a potential metal-ion precursor to realize the homogeneous doping of nanofibers. Among the as-prepared ZZS HNFs, the 15 wt% ZZS HNFs exhibited the highest response, fastest response/recovery time (12/45 s), best selectivity and repeatability, and a detection limit as low as 500 ppb towards HCHO (Fig. 6g–j). The enhancement in the sensing properties of 15 wt% ZZS HNFs could be attributed to the high specific surface area and the increase in oxygen vacancies and chemisorbed oxygen species, benefiting from the homogeneous Zn^{2+} doping and the one-dimensional (1D) nanostructures.

Based on the above cases, the enhanced gas sensing performance caused by metal heteroatoms in resistive gas sensors is mainly attributed to their positive effects on the optimization of the physicochemical properties (including grain size, oxygen vacancy concentration and catalytic activity, *etc.*) of the host materials. Metal heteroatoms can form a large number of surface defects on the surface of the host sensing material and increase the number of chemically active adsorption sites, thereby improving the chemical adsorption capacity toward the targeted gas. Hence, metal heteroatoms can effectively improve the sensitivity of the sensor to the target gas.

3.3. Metal oxides

The introduction of metal oxides into host semiconductor materials has many positive effects, such as introducing more electron depletion layers, improving catalytic activity, increasing adsorption sites, changing the energy band structure and accelerating electron transport, thus achieving high sensitivity and favourable selectivity.[107] Heterojunctions can be formed when metal oxides are combined with other host semiconductor materials, enabling the complementary and synergistic effects of host–guest materials. According to the different conduction types, the heterojunctions can be divided into p–n, n–n and p–p heterojunctions.[31] For the p–n
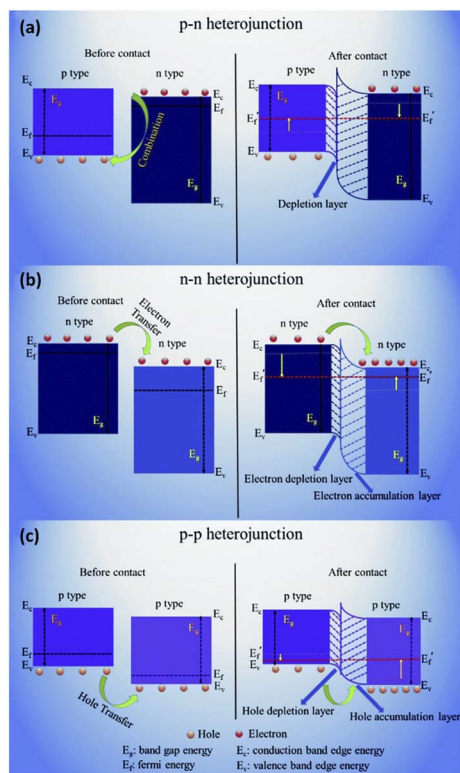
Fig. 7 Schematic illustrations of the energy band structures of different types of heterojunctions: (a) p–n junction, (b) n–n junction and (c) p–p junction. This figure has been reproduced with permission from ref. 31, Royal Society of Chemistry, Copyright 2019.

heterojunction, the electrons at the conduction band move from the n-type semiconductor to the p-type semiconductor, and holes transfer from the p-type semiconductor to the n-type semiconductor until the Fermi level of the nanocomposite reaches equilibrium. Due to the recombination of electrons and holes, an electron depletion layer will be formed at the p–n heterojunction (Fig. 7a). For the n–n heterojunction, electrons will transfer from the high-Fermi level material to the low-Fermi level material at the n–n heterojunction interface, where the semiconductor with a high Fermi level creates a depletion layer and the semiconductor with a low Fermi level forms an accumulation layer (Fig. 7b). For the p–p heterojunction, the holes transfer from a p-type semiconductor with higher valence band energy to another p-type semiconductor with lower valence band energy. Therefore, as shown in Fig. 7c, a cavity depletion zone is formed on the surface of the former (with high valence band energy), while a cavity accumulation zone is formed on the surface of the latter (with low valence band energy).

Kumaresan et al.[108] synthesized nanofibers with the n-WO$_3$/n-TiO$_2$ heterostructure by uniformly loading WO$_3$ nanoparticles (guest) on the TiO$_2$ nanofiber (host) surface through a simple spin coating method. Compared to the original TiO$_2$, n-WO$_3$/n-TiO$_2$ exhibited a more excellent H$_2$ sensing performance. Its response to 1000 ppm H$_2$ at RT was greatly improved from 52.34 to 78.21, and the response/recovery times were also reduced from 42/47 s to 20/23 s. The improved H$_2$-sensing performance of n-WO$_3$/nTiO$_2$ was mainly due to the increase in the gas adsorption sites caused by the heterojunction, the high specific surface area of nanofiber structure, the excellent catalysis effect of WO$_3$ nanoparticles and the Fermi-level effect.

Jayababu et al.[109] synthesized NiO-decorated CeO$_2$ nanostructures via a co-precipitation technique and sol–gel process. The highest response of 1570 (nearly 11 times higher than that of the pure CeO$_2$) was observed for the NiO/CeO$_2$-based gas sensor and sharp response/recovery times (15/19 s) towards 100 ppm isopropanol at RT. The band diagram of the NiO/CeO before and after junction formation is presented in Fig. 8a. After decorating the surface of CeO$_2$ with NiO nanoparticles, the diffusion of electrons and holes from one side to the other side takes place until their Fermi levels become equal. This whole phenomenon develops an internal potential at the interface of the two materials, which is called the built-in potential. The built-in potential at the p-NiO and n-CeO$_2$ interface, as well as the highly catalytic nature and chemical sensitization of decorated NiO, played a vital role in the superior sensing performance of the NiO/CeO$_2$ sensor (Fig. 8b).

Lou et al.[60] designed a highly sensitive and selective formaldehyde sensor based on SnO$_2$/ZnO heterospheres synthesized by atomic layer deposition (ALD). By optimizing the loading of ZnO through changing ALD cycles, the electronic properties at the SnO$_2$/ZnO heterointerface can be modulated. The SnO$_2$/ZnO sensor with ZnO ALD of 10 cycles had the best response/recovery speeds (12/24 s). The SnO$_2$/ZnO sensor also registered a low detection limit of 70 ppb, which allows for the reliable detection of sub-ppm formaldehyde. This remarkable sensor performance indicated that the decoration of metal oxides by ALD surface engineering is promising for the design of host–guest materials.

To date, CPs have been widely used as sensitive materials for the detection of NH$_3$ at RT.[110] Adding metal oxides as guest materials is an effective way to solve the low sensitivity and poor stability of CPs. Li et al.[111] synthesized SnO$_2$-decorated PANI via a combined approach of hydrothermal and in situ polymerization. Compared with the PANI sensor, the 20 mol% SnO$_2$-polyaniline (PASn20) sensor exhibited a 6.2 times higher response (29.8) to 100 ppm NH$_3$ at RT. Furthermore, the PASn20 sensor possessed the ability to detect low NH$_3$ concentrations of 10–200 ppb and a linear response, outstanding selectivity, as well as favorable stability (Fig. 8c–g). The enhanced sensing performance was attributed to the micro-structure with large specific surface area and the formation of the p–n heterojunctions at the surface between PANI and SnO$_2$.

Adopting metal oxides to decorate carbon-based materials can effectively improve the gas sensitivity and achieve fast response/recovery times even under low-temperature conditions, due to the abundance of active sites and a quicker electron transfer benefiting from the well-matched work functions of metal oxides and carbon-based materials.[112] Zhang et al.[113] reported a sub-ppm-level CO gas sensor based on a CuO-decorated rGO hybrid nanocomposite. The CuO/rGO hierarchical nanocomposite was successfully deposited on a substrate with interdigital microelectrodes via a layer-by-layer self-assembly technique. The gas sensing experiment revealed that
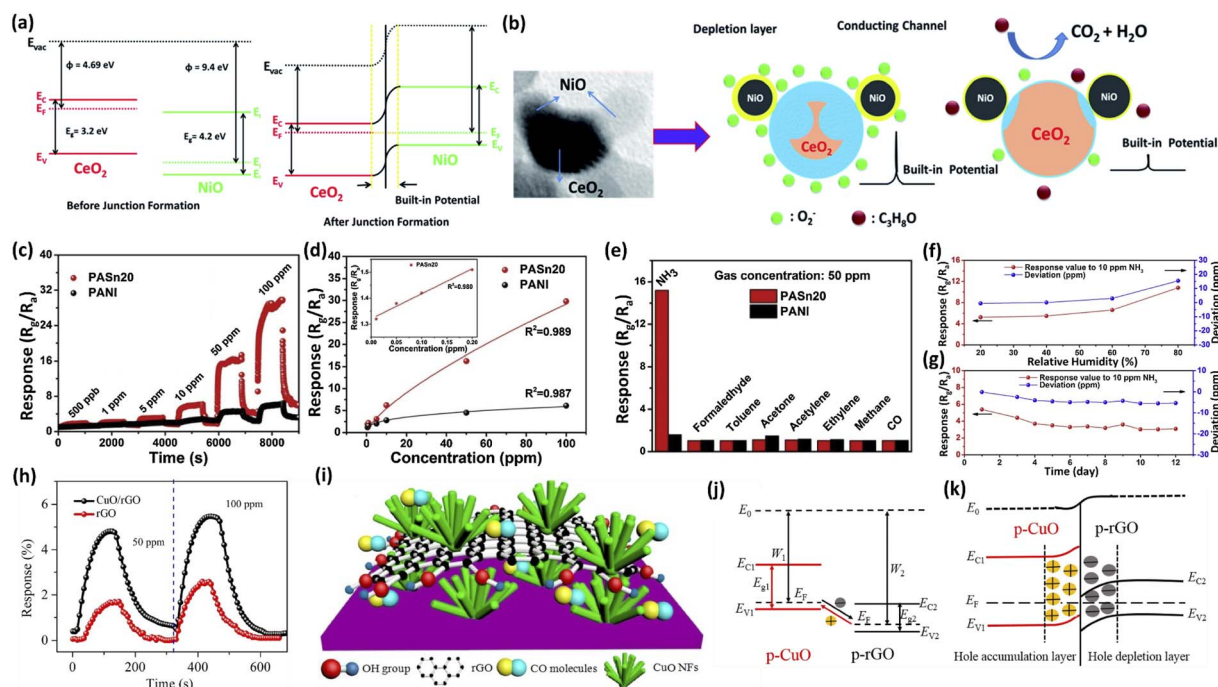
Fig. 8 (a) Schematic diagram demonstrating the band gap alignment of NiO/CeO_2. (b) Schematic illustration of the isopropanol gas sensing mechanism of NiO/CeO_2 gas sensors with surface adsorption and desorption reactions. This figure has been reproduced with permission from ref. 109, Royal Society of Chemistry, Copyright 2019. (c) Dynamic response curves of the sensors based on PANI and PASn20 to various concentrations of NH_3 at 28 °C. (d) The fitting curves of the PANI sensor and PASn20 sensor to NH_3 at 28 °C. (e) The cross-sensitivity of the sensors based on PANI and PASn20 to various testing gases of 50 ppm at 28 °C. (f) The response value of PASn20 at 20−80% RH at 28 °C. (g) Long-term stability of PASn20 at 28 °C. This figure has been reproduced with permission from ref. 111, Elsevier, Copyright 2019. (h) Performance comparison of CO gas sensing between the CuO/rGO nanocomposite sensor and pure rGO film. (i) Schematic of the hybrid nanostructure of CuO/rGO. (j) The energy band diagram of CuO and rGO. (k) The energy band diagram for the p−p junction of the CuO/rGO heterostructure. This figure has been reproduced with permission from ref. 113, Elsevier, Copyright 2019.

the CuO/rGO nanocomposite sensor is capable of sub-ppb-level CO gas detection, good selectivity, fast response/recovery times, acceptable repeatability and stability, which outstripped that of the pure rGO film sensor (Fig. 8h). The enhanced gas sensing properties of the CuO/rGO nanocomposite is ascribed to its hierarchical porous nanostructure and electronic modulation at the interfaces between CuO nanoflowers and rGO nanosheets (Fig. 8i–k).

At RT, the critical drawbacks of the pristine TMD-based gas sensors were their sluggish response and incomplete recoverability due to their lower stability in air or target gas.[114] Decorating MOS on TMDs has attracted significant attention; they not only increase the number of adsorption sites but also provide numerous gas channels and accelerate electron transport. As a result, they have improved sensitivity, stability and recoverability with short response/recovery times. Ikram *et al.*[114] developed rod-like p–n MoS_2–ZnO heterostructures. The ZnO was converted from ZIF-8 by a hydrothermal method. At room temperature, the sensor showed an over 30-fold enhancement in the response compared to the pristine MoS_2 sensor and displayed short response/recovery times while lowering the detection limit of NO_2 to 10 ppb. The sensor retained high stability upon sensing repetition for 10 consecutive weeks. This work demonstrated a facile strategy for the synthesis of p–n MoS_2–ZnO heterostructures for reliable NO_2 gas sensing at RT.

Although the construction of heterostructures will lead to an increased operating temperature in some cases due to a higher activation barrier at the material interfaces, it may be conducive to some specific high-temperature gas sensors.

3.4. Metal–organic frameworks (MOFs)

MOFs are a unique crystalline and porous solid materials composed of metal nodes (metal ions or clusters) and functional organic ligands.[50] MOFs have been investigated extensively for numerous applications (such as gas storage,[115,116] catalysis,[117] and chemical sensors[118–120]) in recent years, due to their large surface areas, tunable pore sizes and abundant functionalizable sites.[50] Nevertheless, many MOFs have relatively low conductivity, meaning that single MOF materials cannot act as host sensing materials for resistive gas sensors. However, the introduction of MOF membranes as guest materials can be considered an ideal solution to solve the issue associated with the poor selectivity of resistive gas sensors.[26,30,121] MOFs with plenty of micropores and active sites can be used as gas molecular probes. Gas molecules can be easily adsorbed and enriched on metal nodes and functional groups in organic ligands, thus improving the sensitivity and reducing the detection limit of gas sensors.[26,122] In addition, MOFs can also be used as molecular sieves due to their

adjustable pore structures. The selective separation of the target gas molecule from the interfering gas can be achieved by a properly designed pore structure.[34]

As shown in Fig. 9a, our group[34] reported an "*in situ* enrichment amplification" (IEA) strategy for constructing the highly sensitive ppb-level HCHO sensor (Fig. 9a). ZIF-8 was coated on electrospun SnO_2 nanofibers by solvothermal reaction and core–shell $ZIF-8-SnO_2$ nanofibers were obtained (Fig. 9b). The screening effect of ZIF-8 helps the small kinetic diameter of formaldehyde (2.43 Å) to easily pass through the small pore aperture of ZIF-8 (3.4 Å), benefiting the selective adsorption for HCHO gas. The IEA-based gas sensors exhibit high sensitivity and selectivity toward the detection of HCHO gas (Fig. 9c and d). The calculated detection limit of the IEA sensor to HCHO gas is 63 ppb, much lower than that of the conventional HCHO sensor (183 ppb). In addition. The validity and universal applicability of the IEA strategy for enhancing gas-sensing properties were verified by using three different materials (SnO_2, In_2O_3, and $LaFeO_3$) as the host materials. All their responses improved significantly after IEA functionalization (Fig. 9e). Therefore, using guest MOFs as enrichment layers is an effective strategy for enhancing the sensitivity of gas sensors.

As mentioned before, Pd is a good H_2-sensitive material, but it has the disadvantage of easy poisoning and deactivation. In addition, the O_2 in air interferes with the detection of H_2 by Pd-based H_2 sensor, depressing the sensitivity and retarding the response/recovery speed. In this regard, Koo *et al.*[123] synthesized ZIF-8 polyhedron particles on lithographically patterned Pd nanowires to construct ZIF-8/Pd NW H_2 sensors. ZIF-8, as a molecular sieving layer, allows the selective penetration of H_2 into Pd-based sensors and effective screening of the relatively larger gas molecules including O_2 (0.346 nm) and N_2 (0.364 nm) in air, thus improving the selectivity of the sensor and significantly reducing the negative effects of air on the sensor (Fig. 9f and g). In addition, the H_2-sensing speed of Pd NWs was dramatically accelerated after the ZIF-8 deposition; the response/recovery times of the ZIF-8/Pd NW sensor to 1% of H_2 were reduced from 164/229 s to 7/10 s.

MOFs can also be composited with a variety of carbon-based materials, and the integration of MOF and carbon-based materials can improve the stability and electrical conductivity. Tung *et al.*[124] used pristine graphene (pG) as the host material and compounded it with three MOF materials (Cu–BTC, UiO-66 and ZIF-8). Graphene with high carrier mobility provided low electrical noise and low power consumption, and the MOFs
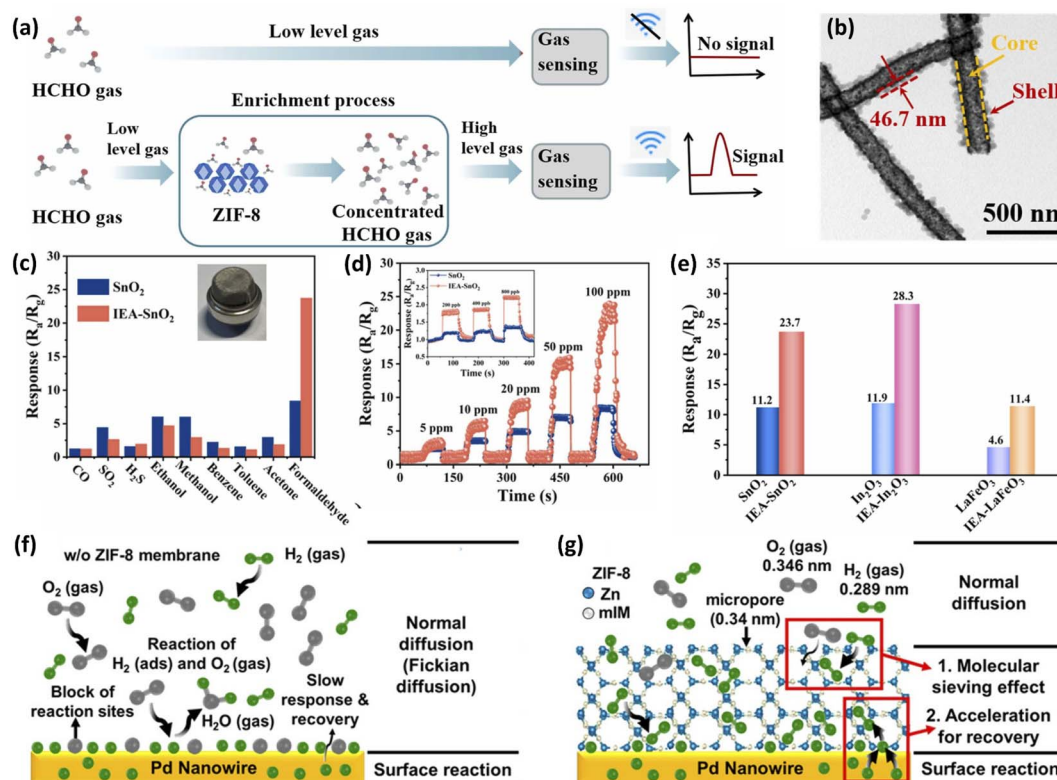

Fig. 9 (a) Schematic illustration of the IEA-based gas sensor. (b) Transmission electron microscope (TEM) image of $ZIF-8-SnO_2$. (c) Responses of sensors to various 100 ppm gases at 300 °C. (d) Dynamic response curves of sensors for different concentrations of HCHO at 300 °C. (e) Responses of different conventional HCHO gas sensors (SnO_2, In_2O_3, and $LaFeO_3$) and the IEA-based sensors (IEA-SnO_2, IEA-In_2O_3, and IEA-$LaFeO_3$) to 100 ppm HCHO. This figure has been reproduced with permission from ref. 34, Elsevier, Copyright 2022. Sensing model for (f) Pd nanowires and (g) Pd nanowires with ZIF-8 membrane. This figure has been reproduced with permission from ref. 119, American Chemical Society, Copyright 2017.

with a high surface area and adsorption capacity provided enhanced sensitivity and selectivity for specific VOCs. All three gas sensors could detect chloroform vapors at the ppm level at RT, and pG–Cu–BTC sensors showed the highest sensitivity and selectivity to chloroform. This was due to the largest specific surface area of Cu–BTC among the three MOFs and the inter-action of chloroform molecules with Cu–BTC leads to increased selectivity.

MOFs can be used as molecular probes and molecular sieves to enhance gas sensing properties (e.g. selectivity, stability and limit of detection). However, some tough problems still exist in the practical application of MOFs. For example, (1) MOFs are generally selective adsorbents only for small molecules of gases. (2) Unmatched design (e.g., an excessively thick MOF-membrane) may block the gas diffusion paths and thus greatly reduce the sensitivity and response recovery speed of gas sensors. (3) When the molecular size of the interfering gases is smaller than or close to the target molecule, it will be difficult to realize high selectivity for the target gases.

3.5. Transition metal dichalcogenides (TMDs)

TMDs are a new kind of semiconductor with high electronic activity, high adsorption capacity and large specific surface area, showing great application prospects in RT gas sensors. The functional mechanism of TMDs guest materials is mainly based on the construction of heterojunctions, enhancement of charge transfer, synergistic effects and complementary advantages, similar to that of metal oxides. 2D TMDs suffer from the disad-vantage of easy agglomeration, however, it can be effectively overcome after appropriate modification by some functional guest materials. MOSs modified with 2D TMDs can suppress the agglomeration of the MOSs and improve electrical conductivity, thereby improving the gas sensing performance.[125]

MoS_2 is the leading application in the field of gas sensing, and its composites with MOSs are also widely used in gas detection applications. Ding et al.[126] synthesized Cu_2O nanoparticles decorated with MoS_2 nanosheets via a facile hydrothermal and wet chemical method. Under an optimal low-operating temper-ature of 75 °C, the response of the p–p Cu_2O/MoS_2 sensor (872%) with an optimized composition for 100 ppm NH_3 increased by more than 8 times as compared with the pristine Cu_2O (103%). The Cu_2O/MoS_2 sensor also exhibited excellent selectivity for NH_3 against other interferent gases. The enhanced sensing property of the nanohybrid benefits from the superimposed effect of the p–p heterojunction formation and the elevated specific surface area at the interface between Cu_2O and MoS_2.

Chang et al.[127] introduced MoS_2 nanosheets on the surface of p-type ZnO derived from ZIF-8 to produce ZnO@MoS_2 core/shell heterojunctions as a novel acetone sensor. The ZnO@MoS_2 exhibited an enhancement of about 80 times in response to 100 ppb acetone compared that of pure ZnO (Fig. 10a). More importantly, this ZnO@MoS_2 heterojunction sensor exhibited an ultra-fast response/recovery (60/40 s) to acetone of ultra-low concentration (5 ppb). Moreover, the acetone sensing perfor-mance is negligibly affected by humidity and other gases, which is suitable for exhaled acetone detection (Fig. 10b and c). The
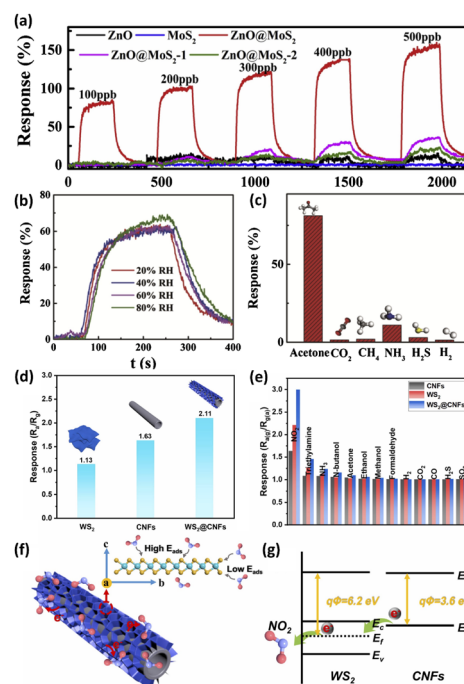

Fig. 10   (a) Dynamic response curves of the ZnO and MoS_2-based sensor to 100–500 ppb acetone at 350 °C. (b) The sensing charac-teristics of the ZnO@MoS_2 sensor towards 100 ppb acetone under different relative humidity levels. (c) The response of the ZnO@MoS_2 sensor to 100 ppb acetone, 250 ppm CO_2, 250 ppm CH_4, 5 ppm NH_3, 5 ppm H_2S, and 250 ppm H_2. This figure has been reproduced with permission from ref. 123, Elsevier, Copyright 2020. (d) The response of CNFs, WS_2, and WS_2@CNFs to 10 ppm of NO_2 at RT. (e) Selectivity of CNFs, WS_2, and WS_2@CNFs to 50 ppm of various gases. (f) Schematic illustration of the sensing mechanism of WS_2@CNFs. (g) Band diagram for WS_2@CNFs. This figure has been reproduced with permission from ref. 124, Elsevier, Copyright 2021.

sharp increase in the negative heterojunction interface resis-tance, ultra-fast gas diffusion rates in MoS_2 nanosheets and strong interaction energy are key factors for the excellent acetone sensing properties of ZnO@MoS_2.

The edges of TMDs have high adsorption capability and electronic activity. The exposure of the edges of TMDs remains a great obstacle to achieving high sensor sensitivity. Loading TMDs onto carbon-based materials is an effective method. In an attempt to increase the exposure of the edges of TMDs to improve the gas sensing properties, Xu et al.[128] demonstrated a high-performance RT NO_2 gas sensor based on WS_2 nanosheets/carbon nanofibers (CNFs) composite few-layer WS_2 nanosheets anchored on CNFs through a hydrothermal process. This process achieved a coating presenting an optimized active surface area and accessibility of the sensing layers. The expo-sure of WS_2 edges remarkably improved the sensing properties. Consequently, the WS_2@CNFs composite exhibited excellent selectivity for NO_2 at RT with improved response, good selec-tivity and much lower detection limit in comparison to the CNFs (Fig. 10d and e). The improved response and selectivity are due to the synergistic contribution from the WS_2 edge-rich structure and high conductivity of CNFs (Fig. 10f and d). Density

functional theory (DFT) calculations verified that the edge sites of WS_2 were more beneficial for NO_2 adsorption with improved electron transfer as compared to the basal surface of WS_2.

3.6. Polymers

CPs, as guest materials used in resistive gas sensors, have many unique advantages benefiting from their excellent electronic properties, low operating temperatures and intrinsic redox reactivity. CPs can form heterojunctions with the host gas sensing materials to enhance electron transport. In addition, some groups on CPs can react with specific gas molecules, thus increasing selectivity and sensitivity to those gases.[129]

For example, Guo et al.[57] developed a hierarchically nano-structured rGO–PANI composite film. The assembled flexible, transparent electronic gas sensor exhibited favorable
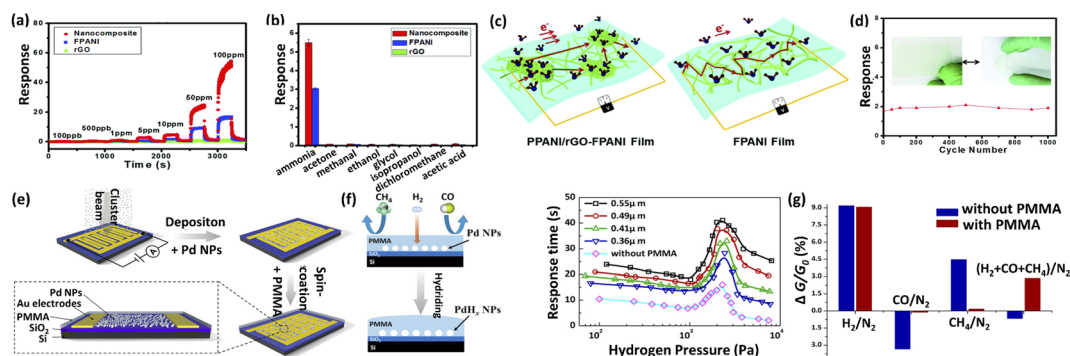

Fig. 11 (a) Sensing performances with different concentrations of NH_3 ranging from 100 ppb to 100 ppm for the rGO film, the PANI and the rGO–PANI. (b) Gas sensing selectivity (averaged results with error bars) of the rGO, PANI and the rGO–PANI for various volatile gases. (c) The proposed mechanisms of charge transport for the rGO–PANI and PANI. (d) The investigation of the flexibility of the transparent sensors by measuring the sensing performances in the bent and extended states (5 ppm NH_3). This figure has been reproduced with permission from ref. 57, Royal Society of Chemistry, Copyright 2016. (e) Schematic illustration of the procedure used to fabricate the hydrogen sensor based on a PMMA-membrane-coated Pd NP film. (f) Schematic illustration of the sensing kinetics of PMMA-Pd and plots of the response time versus the thickness of the PMMA membrane layer. (g) The response of sensors with and without a PMMA membrane layer to target gas mixtures including CO/N_2, CH_4/N_2, H_2/N_2, and $(H_2 + CO + CH_4)/N_2$. This figure has been reproduced with permission from ref. 127, American Chemical Society, Copyright 2017.
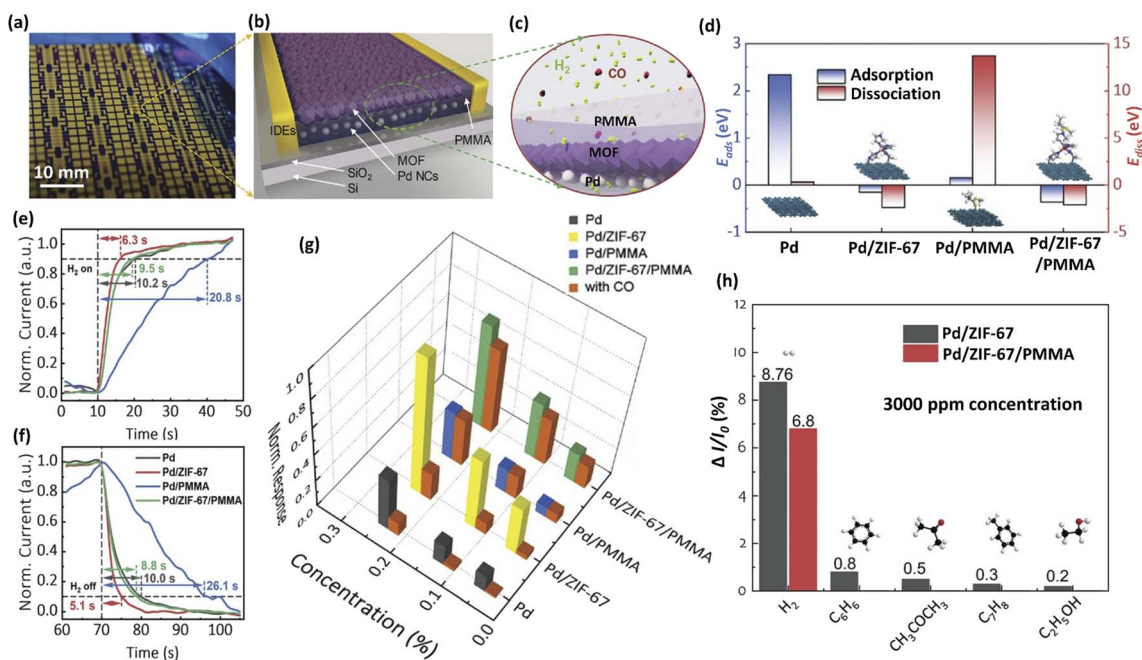
Fig. 12 (a–c) The prototype and concept of the Pd/MOF/PMMA nanocomposite-based H_2 sensor. (d) Calculated adsorption and dissociation energies for Pd, Pd/ZIF-67, Pd/PMMA, and Pd/ZIF-67/PMMA. (e) Response and (f) recovery curves of Pd, Pd/ZIF-67, Pd/PMMA, and Pd/ZIF-67/PMMA-based sensors. (g) Comparison of normalized response amplitudes at 0.05%, 0.13%, and 0.24% H_2 concentrations with and without 1% CO for all four samples. (h) Selective sensing performance of the Pd/ZIF-67 and Pd/ZIF-67/PMMA sensors against various VOCs at 3000 ppm. This figure has been reproduced with permission from ref. 92, Wiley, Copyright 2012.

performance, such as high sensitivity and linear responses towards NH_3 gas concentrations ranging from 100 ppb to 100 ppm, as well as outstanding selectivity (Fig. 11a). The fast electron transfer between hybrids and NH_3, assisted by $\pi-\pi$ interactions of PANI and rGO with a low electron transfer energy barrier, led to more electron transfer from PANI to rGO, thus effectively improving the responsivity and response speed (Fig. 11c). In addition, the rGO–PANI sensor showed satisfactory flexibility and stability (Fig. 11d). Sonker et al.[130] synthesized TiO_2–PANI nanofilm by spin-coating technology for enabling

the CO_2 gas sensor to operate at RT conditions. In addition to the formation of enough active sites on the surface of TiO_2, the uniformly dispersed 1% PANI particles in TiO_2 (TiO_2–PANI (1%)) could also change the electron Debye length and enhance the chemical adsorption, hence realizing the excellent CO_2 sensing performance (53–1000 ppm CO_2 gas) at RT. Han et al.[129] fabricated a polyethyleneimine (PEI)-functionalized CNT sensor for CO_2 detection at RT. Uniform CNT thin films prepared by a filtration method were used as resistive networks. The abundant amino group in PEI could react with CO_2 to form

Table 1 Summary of resistive gas sensors functionalized by different kinds of guest materials (noble metals, metal heteroatoms, metal oxides, MOF, TMD, polymers, and multiple guest materials)

Type of guest material	Host–guest material	Target gas	Performance					
			Concentration	Response	$T_{response}/T_{recvoery}$ (s)	Temperature (°C)	Limit of detection	Ref.
Noble metal	WO_3–Ag	NO_2	5 ppm	90.3	—	225	0.5 ppm	89
	WO_3–Pd	H_2	500 ppm	22 867	1.2/77	50	5 ppm	135
	WO_3–Ru	Ethanol	100 ppm	120	—	200	221 ppb	136
	Co_3O_4–Au	Acetone	100 ppm	14.5	319/280	190	1 ppm	90
	Co_3O_4–Pd	Ethanol	100 ppm	24	12/25	150	—	67
	TiO_3–Pd	H_2	1000 ppm	9	1.6/1.4	230	1 ppm	93
	CNT–Pt	Toluene	5 ppm	5.06	80/90	150	1 ppm	85
	Graphene–Pd	H_2	40 ppm	55%	6/23	RT	—	96
	MoS_2–Pt	H_2	1%	8	8.1/16	RT	—	97
	WSe_2–Pd	CO	5 ppm	9.25	52/97	RT	1 ppm	98
Metal heteroatom	In_2O_3–Al	HCHO	100 ppm	60.3	2/—	150	60 ppb	104
	In_2O_3–Ca	Ethanol	100 ppm	183.3	2/56	240	5 ppm	105
	ZnO–Al	CO	80 ppm	74	21/70	250	250 ppb	106
	SnO_2–Zn	HCHO	100 ppm	25.7	12/45	400	500 ppb	22
	In_2O_3–Sn	HCHO	100 ppm	24.5	2.6/79.4	160	—	137
Metal oxide	TiO_2–WO_3	H_2	1000 ppm	78.21	20/23	RT	—	108
	CeO_2–NiO	Isopropanol	100 ppm	1570	15/19	RT	1	109
	SnO_2–ZnO	HCHO	1 ppm	9.7	12/24	200	70 ppb	60
	SnO_2–CuO	Toluene	75 ppm	540	100/36	400	—	138
	$Bi_2Mo_3O_{12}$–Co_3O_4	Ethanol	100 ppm	30.25	34/26	170	1 ppm	139
	PANI–SnO_2	NH_3	100 ppm	29.8	125/167	RT	10 ppb	111
	rGO/CuO	CO	1 ppm	2.56	70/160	RT	250 ppb	113
	$MWCNT/SnO_2$	H_2S	50 ppm	108	23/44	70	43 ppb	140
	MoS_2–ZnO	NO_2	50 ppm	35	1.5/30.9	RT	10 ppb	114
MOF	SnO_2-ZIF-8	HCHO	100 ppm	23.7	2/26	300	63 ppb	34
	ZnO-ZIF-8	HCHO	100 ppm	12.5	16/9	300	5.6 ppm	141
	ZnO-ZIF-71	Ethanol	50 ppm	320%	—	250	—	142
	SnO_2-ZIF-67	CO_2	5000 ppm	16.5	10/25	205	—	143
	Pd-ZIF-8	H_2	1%	3.5	7/10	RT	0.06%	123
	Graphene–Cu–BTC	Chloroform	22.6 ppm	2.5	—	RT	2.82 ppm	124
TMD	Cu_2O–MoS_2	NH_3	100 ppm	872%	—	RT	—	126
	ZnO–MoS_2	Acetone	500 ppb	150%	9/17	350	5 ppb	127
	ZnO–$MoSe_2$	H_2	500 ppm	60	19/40	RT	1 ppm	144
	CNF–WS_2	NO_2	10 ppm	6.9	23/94	150	31 ppb	128
Polymer	rGO–PANI	NH_3	10 ppm	8	36/18	RT	100 ppb	57
	TiO_2–PANI	CO_2	1000 ppm	53	552/342	RT	—	130
	CNT–PEI	CO_2	1000 ppm	4.2	—	RT	—	129
	GO–PPy	CO	300	45	89/95	RT	—	145
	Pd–PMMA	H_2	1000 ppm	9	22.84/—	RT	50 ppm	131
Multiple	Pd-ZIF-67-PMMA	H_2	1%	25	9.5/8.8	RT	—	92
	ZnO–Ag–MoS_2	CO	100 ppm	5	40/50	RT	1 ppm	132
	ZnO–Au-ZIF-8	HCHO	100 ppm	70	—	RT	250 ppb	134
	ZnO–Ag–In_2O_3	HCHO	100 ppm	186	10/67	260	9 ppb	133
	TiO_2–$CoTiO_3$–Pd	Benzene	50 ppm	33.46	49/9	RT	100 ppb	73

carbamate at RT, giving PEI-CNT a better sensing performance than the original CNT.

In addition to CPs, non-conductive polymers can also serve as functional guest materials for use in resistive gas sensors. Coating with a polymeric membrane for screening out interfering gases is a feasible approach to fabricating gas sensors with high selectivity. They can also act as protective layers against the poisoning and inactivation of the host materials, thereby improving the stability of gas sensors. Chen *et al.*[131] fabricated polymethyl methacrylate (PMMA) membrane-coated Pd nanoparticle films for high-performance H_2 gas sensors by carrying out gas-phase cluster deposition and PMMA spin coating (Fig. 11e). After PMMA coating, the sensor response decreased slightly, but the selectivity for hydrogen increased significantly (Fig. 11f and g). However, the device sensing kinetics were strongly affected by the thickness of the PMMA layer, with the devices with thicker PMMA membrane layers showing a slower response to H_2 gas (Fig. 11f).

3.7. Multiple guest materials

Although the above guest materials (noble metals, metal heteroatoms, metal oxides, MOFs, TMDs and polymers) have many advantages and can significantly improve the gas sensing properties, there are still some problems (*e.g.* poor stability, easy poisoning and inactivation, insufficient sensitivity and selectivity) that hinder the practical application of these materials. In many cases, adding two or more guest materials can ameliorate these defects and dramatically improve the sensitivity.[30]

To solve the toxic inactivation of Pd-based sensors, Xie *et al.*[92] proposed a hybrid H_2 sensor consisting of Pd nanocluster film, MOF, and polymer (Fig. 12a–c). The PMMA coating, as a protection layer, endows the sensor with excellent H_2 selectivity and CO poisoning resistance. The ZIF-67 serves as an interface layer between the Pd film and the polymer layer, which alters the nature of the interaction with hydrogen and leads to significant sensing performance improvements, owing to the interfacial electronic coupling between Pd NCs and the MOF. The strategy overcomes the shortcomings of retarded response speed and degraded sensitivity induced by the polymer coating of a Pd film-polymer hybrid system. Pd/ZIF-67/PMMA had both lower adsorption and analytical energy, thus exhibiting faster response/recovery (Fig. 12d–f). As shown in Fig. 12g, compared with the pristine Pd sensor, Pd/ZIF-67 showed a higher response but poor poisoning resistance, while Pd/PMMA had good poisoning resistance but a reduced response. Pd/ZIF-67/PMMA exhibited both high sensitivity and poisoning resistance even with excellent selectivity (Fig. 12h).

When the heterojunction was combined with noble metal catalysts, its sensing properties can be greatly enhanced. Zhang *et al.*[132] prepared a new ternary nanocomposite of Ag–ZnO/MoS$_2$ *via* a layer-by-layer (LbL) self-assembly method for carbon monoxide (CO) sensing application. The Ag–ZnO/MoS$_2$ nanocomposite sensor has excellent response, swift response/recovery characteristics, as well as acceptable repeatability and selectivity, which outstripped the pure ZnO and ZnO/MoS$_2$ sensors. The underlying sensing mechanism of the Ag–ZnO/ MoS$_2$ nanocomposite film was attributed to the catalytic activity of Ag and the synergistic effect of ZnO and MoS$_2$. Liu *et al.*[133] fabricated a high-response formaldehyde gas sensor based on Ag–ZnO/In$_2$O$_3$ nanofibers. The Ag–ZnO/In$_2$O$_3$ exhibited superior sensitivity, low detection limit (9 ppb), excellent selectivity and durable stability (the deviation value $\leq 3\%$). Particularly, an ultra-high response value of about 186 towards 100 ppm of formaldehyde at 260 °C was achieved. The enhanced gas sensing properties can be mainly attributed to multi-level heterojunctions (n–n heterojunction and ohmic junction) and the spill-over effect of Ag, ultimately increasing the adsorption of gas molecules on the surface of the sensing material.

Wang *et al.*[134] synthesized Au@ZnO@ZIF-8 *via* an anisotropic growth method for the simultaneous detection and removal of formaldehyde at RT. Due to the synergistic effects of the high conductivity of ZnO, the superior gas adsorption capability of ZIF-8, the clean interface between ZnO and ZIF-8, and the plasmonic resonance of gold nanorods, the Au@ZnO@ZIF-8 demonstrated an excellent sensing performance with a selective detection toward formaldehyde at RT. Au@ZnO@ZIF-8 hybrids had enhanced selective adsorption, detection and oxidation of HCHO and prevented interference from gases such as H_2O and toluene, where Au helped to generate charge carriers on a ZnO surface under visible-light irradiation.

Herein, we have further summarized the previously reported gas sensors based on different kinds of guest materials (noble metals, metal heteroatoms, metal oxides, MOF, TMD, polymers and multiple guest materials), as shown in Table 1.

4. Conclusions and perspectives

In this review, the functions, working mechanisms, and advantages/disadvantages of seven commonly-used guest materials (noble metals, metal heteroatoms, metal oxides, MOFs, TMDs, polymers and multiple guest materials) in resistive gas sensors are discussed in detail. Resistive gas sensors have been considered attractive candidates for gas detection due to their fast response/recovery, ease of operation, low cost, and good portability. To date, plenty of gas-sensitive materials (represented by MOSs) have been developed. The shortcomings of these materials make it difficult for them to meet the needs of practical applications. For example, MOSs endure high operating temperatures and poor selectivity; CPs suffer from poor stability and low sensitivity; carbon-based materials have the problems of poor reversibility; TMDs tend to agglomerate and self-stack, and oxidize easily in air. To solve these problems and obtain better gas-sensitive properties, it is necessary to introduce functional guest materials. Guest materials can functionalize the host material by introducing catalytic sites, promoting charge transfer, improving carrier transport, and/or introducing protective/sieving/enrichment layers. Guest materials can also produce synergistic effects and complementary advantages with the host materials, thereby effectively improving the sensitivity, selectivity and stability of the gas sensors. However, the introduction of guest materials will also cause some negative problems in some cases. Fig. 13 shows the merits and demerits of the functional guest materials in detail.

Fig. 13 The merits and demerits of the functional guest materials.

With the development of industrialization, environmental problems are receiving more and more attention. To improve the performance of resistive gas sensors, the introduction of functional guest materials has become an inevitable trend. Although some progress has been made in the preparation of high-performance resistive gas sensors based on various guest materials, current research still faces some challenges that need to be further addressed:

(1) Gas sensors that operate under low energy consumption and room-temperature conditions are receiving ever-increasing attention. Some emerging 2D materials (such as TMDs, rGO, 2D-conductive-MOFs, and MXenes) show great potential in this area and have great application prospects after optimization by guest materials.

(2) For most host–guest hybrid materials, the control of the synthesis process (such as the doping amount, thickness of the load film, aperture control, *etc.*) has a great influence on the gas sensor performance. Hence, it may be necessary to focus more attention on the influencing mechanism of these key parameters rather than focusing only on gas-sensitive materials themselves.

(3) The modification of guest materials can greatly improve the performance of the host materials but the current research on the mechanism is not in-depth. Interpretations of their sensing mechanisms are mainly based on the speculation of experimental results. It is necessary to explore the gas sensitivity mechanisms at a deeper level through *in situ* characterization tests combined with theoretical calculations and simulation.

(4) It is difficult for a single gas sensor to meet the requirements of multi-component mixed gas detection in the fields of

human exhaled disease diagnosis and atmospheric gas pollutant monitoring. Therefore, a sensor array (e-nose) composed of multiple sensor units is needed to further improve the accuracy of gas detection combined with intelligent algorithms.

Author contributions

Jianan Wang conceived and designed the work; Ze Wang wrote the manuscript; Jianan Wang, Lei Zhu, Rui Zhuang, Pengfei Mu and W. Yan revised the manuscript. Ze Wang and Jingzhao Wang arranged the figures. All authors have given approval to the final version of the manuscript.

Conflicts of interest

There are no conflicts to declare.

Abbreviations

MOSs	Metal oxide semiconductors
CPs	Conductive polymers
MOFs	Metal–organic frameworks
PPy	Polypyrrole
PTh	Polythiophene
PANI	Polyaniline
TMDs	Transition metal dichalcogenides
IDE	Interdigitated electrode
MEMS	Micro-Electro-Mechanical System
PET	Polyethylene-terephthalate
PI	Polyimide
GO	Graphene oxide
rGO	Reduced graphene oxide
CNT	Carbon nanotube
SWCNT	Single wall carbon nanotube
MWCNTs	Multi-walled carbon nanotubes
ZZS HNFs	Zn^{2+}-doped SnO_2 hollow nanofibers
CNFs	Carbon nanofibers
1D	One-dimensional
2D	Two-dimensional
3D	Three-dimensional
IEA	*In situ* enrichment amplification
PMMA	Polymethyl methacrylate
pG	Pristine graphene
TEM	Transmission electron microscope
RT	Room temperature
VOCs	Volatile organic compounds
ALD	Atomic layer deposition
LbL	Layer-by-layer
DFT	Density functional theory
PEI	Polyethyleneimine

Acknowledgements

References

1 J. van den Broek, S. Abegg, S. E. Pratsinis and A. T. Guntner, *Nat. Commun.*, 2019, **10**, 4220.

2 F. Zhang, Q. Lin, F. Han, Z. Wang, B. Tian, L. Zhao, T. Dong and Z. Jiang, *Microsyst. Nanoeng.*, 2022, **8**, 40.

3 Y. Zhang, J. Zhao, T. Du, Z. Zhu, J. Zhang and Q. Liu, *Sci. Rep.*, 2017, **7**, 1960.

4 W. Liu, L. Xu, K. Sheng, X. Zhou, B. Dong, G. Lu and H. Song, *NPG Asia Mater.*, 2018, **10**, 293–308.

5 G. S. Kulkarni, K. Reddy, Z. Zhong and X. Fan, *Nat. Commun.*, 2014, **5**, 4376.

6 S. Jiang and Y. Liu, *TrAC, Trends Anal. Chem.*, 2020, **126**, 115877.

7 P. F. M. Pereira, P. H. de Sousa Picciani, V. Calado and R. V. Tonon, *Trends Food Sci. Technol.*, 2021, **118**, 36–44.

8 L. Zhu and W. Zeng, *Sens. Actuators, A*, 2017, **267**, 242–261.

9 R. Malik, V. K. Tomer, Y. K. Mishra and L. Lin, *Appl. Phys. Rev.*, 2020, **7**, 021301.

10 H. Nazemi, A. Joseph, J. Park and A. Emadi, *Sensors*, 2019, **19**, 1258.

11 S. Akshya and A. V. Juliet, *Sci. Rep.*, 2021, **11**, 970.

12 D. Del Orbe Henriquez, I. Cho, H. Yang, J. Choi, M. Kang, K. S. Chang, C. B. Jeong, S. W. Han and I. Park, *ACS Appl. Nano Mater.*, 2020, **4**, 7–12.

13 D. Tyagi, H. Wang, W. Huang, L. Hu, Y. Tang, Z. Guo, Z. Ouyang and H. Zhang, *Nanoscale*, 2020, **12**, 3535–3559.

14 D. Popa and F. Udrea, *Sensors*, 2019, **19**, 2076.

15 J. Y. Monter-Guzmán, X. Chu, E. Comini, M. Epifani and R. Zanella, *Chemosensors*, 2021, **9**, 193.

16 Z. Yang, L. Jiang, J. Wang, F. Liu, J. He, A. Liu, S. Lv, R. You, X. Yan, P. Sun, C. Wang, Y. Duan and G. Lu, *Sens. Actuators, B*, 2021, **326**, 128828.

17 T. Lin, X. Lv, Z. Hu, A. Xu and C. Feng, *Sensors*, 2019, **19**, 233.

18 Z. Wang, L. Zhu, S. Sun, J. Wang and W. Yan, *Chemosensors*, 2021, **9**, 198.

19 L. Zhu, J. Wang, J. Liu, X. Chen, Z. Xu, Q. Ma, Z. Wang, J. Liang, S. Li and W. Yan, *Appl. Surf. Sci.*, 2022, **590**, 153085.

20 Z. Wang, L. Zhu, J. Liu, J. Wang and W. Yan, *Energy Fuels*, 2022, **36**, 6038–6057.

21 G. Neri, *Chemosensors*, 2015, **3**, 1–20.

22 L. Zhu, J. Wang, J. Liu, M. S. Nasir, J. Zhu, S. Li, J. Liang and W. Yan, *Sens. Actuators, B*, 2021, **326**, 128819.

23 V. Schroeder, S. Savagatrup, M. He, S. Lin and T. M. Swager, *Chem. Rev.*, 2019, **119**, 599–663.

24 H. Cruz-Martinez, H. Rojas-Chavez, F. Montejo-Alvaro, Y. A. Pena-Castaneda, P. T. Matadamas-Ortiz and D. I. Medina, *Sensors*, 2021, **21**, 1992.

25 C.-C. Lin, S. Gupta, C. Chang, C.-Y. Lee and N.-H. Tai, *Mater. Lett.*, 2021, **297**, 129941.

26 W.-T. Koo, J.-S. Jang and I.-D. Kim, *Chem*, 2019, **5**, 1938–1963.

27 C. Dong, R. Zhao, L. Yao, Y. Ran, X. Zhang and Y. Wang, *J. Alloys Compd.*, 2020, **820**, 153194.

28 D. Zhang, S. Yu, X. Wang, J. Huang, W. Pan, J. Zhang, B. E. Meteku and J. Zeng, *J. Hazard. Mater.*, 2022, **423**, 127160.

29 Z. Li, X. Liu, M. Zhou, S. Zhang, S. Cao, G. Lei, C. Lou and J. Zhang, *J. Hazard. Mater.*, 2021, **415**, 125757.

30 Y. Jian, W. Hu, Z. Zhao, P. Cheng, H. Haick, M. Yao and W. Wu, *Nano-Micro Lett.*, 2020, **12**, 71.

31 Z. Li, H. Li, Z. Wu, M. Wang, J. Luo, H. Torun, P. Hu, C. Yang, M. Grundmann, X. Liu and Y. Fu, *Mater. Horiz.*, 2019, **6**, 470–506.

32 H. Yuan, N. Li, W. Fan, H. Cai and D. Zhao, *Adv. Sci.*, 2022, **9**, 2104374.

33 F. A. A. Nugroho, I. Darmadi, L. Cusinato, A. Susarrey-Arce, H. Schreuders, L. J. Bannenberg, A. B. da Silva Fanta, S. Kadkhodazadeh, J. B. Wagner, T. J. Antosiewicz, A. Hellman, V. P. Zhdanov, B. Dam and C. Langhammer, *Nat. Mater.*, 2019, **18**, 489–495.

34 L. Zhu, J. Wang, J. Liu, Z. Xu, M. S. Nasir, X. Chen, Z. Wang, S. Sun, Q. Ma, J. Liu, J. Feng, J. Liang and W. Yan, *Sens. Actuators, B*, 2022, **354**, 131206.

35 W. H. Brattain and J. Bardeen, *Bell Syst. Tech. J.*, 1954, **32**, 1–41.

36 T. Seiyama and A. Kato, *Anal. Chem.*, 1962, **34**, 1502–1503.

37 P. J. Shaver, *Appl. Phys. Lett.*, 1967, **11**, 255–257.

38 C. Nylander, M. Armgarth and L. Lundstrom, *Anal. Chem. Symp. Ser.*, 1983, **17**, 203–207.

39 F. Schedin, A. K. Geim, S. V. Morozov, E. W. Hill, P. Blake, M. I. Katsnelson and K. S. Novoselov, *Nat. Mater.*, 2007, **6**, 652–655.

40 Y. P. Sun, K. F. Fu, Y. Lin and W. J. Huang, *Acc. Chem. Res.*, 2002, **35**, 1096–1104.

41 D. Wang, S. M. Huang, H. J. Li, A. Y. Chen, P. Wang, J. Yang, X. Y. Wang and J. H. Yang, *Sens. Actuators, B*, 2019, **282**, 961–971.

42 J. N. Chang, H. J. Zhang, J. L. Cao and Y. Wang, *Adv. Powder Technol.*, 2022, **33**, 103432.

43 J. S. Kim, H. W. Yoo, H. O. Choi and H. T. Jung, *Nano Lett.*, 2014, **14**, 5941–5947.

44 K. Rathi and K. Pal, *Adv. Mater. Interfaces*, 2020, **7**, 2000140.

45 J. H. Kim, J. Y. Kim, A. Mirzaei, H. W. Kim and S. S. Kim, *Sens. Actuators, B*, 2021, **332**, 129493.

46 H. J. Zhang, F. N. Meng, L. Z. Liu, Y. J. Chen and P. J. Wang, *J. Alloys Compd.*, 2018, **764**, 147–154.

47 X. L. Yang, S. F. Zhang, Q. Yu, P. Sun, F. M. Liu, H. Y. Lu, X. Yan, X. Zhou, X. S. Liang, Y. Gao and G. Y. Lu, *Sens. Actuators, B*, 2018, **270**, 538–544.

48 B. Y. Zong, Q. K. Xu, Q. J. Li, X. Fang, X. Y. Chen, C. B. Liu, J. B. Zang, Z. Bo and S. Mao, *J. Mater. Chem. A*, 2021, **9**, 14411–14421.

49 D. Wang, D. Zhang, Y. Yang, Q. Mi, J. Zhang and L. Yu, *ACS Nano*, 2021, **15**, 2911–2919.

50 H. Y. Li, S. N. Zhao, S. Q. Zang and J. Li, *Chem. Soc. Rev.*, 2020, **49**, 6364–6401.

51 J. Zhang, X. H. Liu, G. Neri and N. Pinna, *Adv. Mater.*, 2016, **28**, 795–831.

52 J. F. Fennell, S. F. Liu, J. M. Azzarelli, J. G. Weis, S. Rochat, K. A. Mirica, J. B. Ravnsbaek and T. M. Swager, *Angew. Chem., Int. Ed.*, 2016, **55**, 1266–1281.

53 S. Li, L. Xie, M. He, X. Hu, G. Luo, C. Chen and Z. Zhu, *Sens. Actuators, B*, 2020, **310**, 127828.

54 J. Wang, Q. Zhou, Z. Wei, L. Xu and W. Zeng, *Ceram. Int.*, 2020, **46**, 29222–29232.

55 N. Yi, Z. Cheng, H. Li, L. Yang, J. Zhu, X. Zheng, Y. Chen, Z. Liu, H. Zhu and H. Cheng, *Mater. Today Phys.*, 2020, **15**, 100265.

56 R. You, D.-D. Han, F. Liu, Y.-L. Zhang and G. Lu, *Sens. Actuators, B*, 2018, **277**, 114–120.

57 Y. Guo, T. Wang, F. Chen, X. Sun, X. Li, Z. Yu, P. Wan and X. Chen, *Nanoscale*, 2016, **8**, 12073–12080.

58 B. Behera and S. Chandra, *Sens. Actuators, B*, 2016, **229**, 414–424.

59 D. Meng, J. P. Si, M. Y. Wang, G. S. Wang, Y. B. Shen, X. G. San and F. L. Meng, *Chin. Chem. Lett.*, 2020, **31**, 2133–2136.

60 C. Lou, C. Yang, W. Zheng, X. Liu and J. Zhang, *Sens. Actuators, B*, 2021, **329**, 129218.

61 M. K. Filippidou, M. Chatzichristidi and S. Chatzandroulis, *Sens. Actuators, B*, 2019, **284**, 7–12.

62 A. Nag, S. C. Mukhopadhyay and J. Kosel, *IEEE Sens. J.*, 2017, **17**, 3949–3960.

63 Z. Q. Zheng, J. D. Yao, B. Wang and G. W. Yang, *Sci. Rep.*, 2015, **5**, 11070.

64 Z. Q. Zheng, J. D. Yao, B. Wang and G. W. Yang, *Nanotechnology*, 2017, **28**, 415501.

65 P. M. Perillo and D. F. Rodriguez, *J. Alloys Compd.*, 2016, **657**, 765–769.

66 S. M. Majhi, A. Mirzaei, H. W. Kim, S. S. Kim and T. W. Kim, *Nano Energy*, 2021, **79**, 105369.

67 G. Yuan, Y. Zhong, Y. Chen, Q. Zhuo and X. Sun, *RSC Adv.*, 2022, **12**, 6725–6731.

68 T. J. Hsueh and S. S. Wu, *Sens. Actuators, B*, 2021, **329**, 129201.

69 L. F. Zhu, J. C. She, J. Y. Luo, S. Z. Deng, J. Chen, X. W. Ji and N. S. Xu, *Sens. Actuators, B*, 2011, **153**, 354–360.

70 I. D. Kim, A. Rothschild and H. L. Tuller, *Acta Mater.*, 2013, **61**, 974–1000.

71 T. He, W. Liu, T. Lv, M. Ma, Z. Liu, A. Vasiliev and X. Li, *Sens. Actuators, B*, 2021, **329**, 129275.

72 X. Yang, S. Zhang, Q. yu, L. Zhao, P. Sun, T. Wang, F. Liu, X. Yan, Y. Gao, X. Liang, S. Zhang and G. Lu, *Sens. Actuators, B*, 2019, **281**, 415–423.

73 D. Wang, D. Zhang and Q. Mi, *Sens. Actuators, B*, 2022, **350**, 130830.

74 M. Liu, Z. Wang, P. Song, Z. Yang and Q. Wang, *Sens. Actuators, B*, 2021, **340**, 129946.

75 J. Lee, Y. Jung, S.-H. Sung, G. Lee, J. Kim, J. Seong, Y.-S. Shim, S. C. Jun and S. Jeon, *J. Mater. Chem. A*, 2021, **9**, 1159–1167.

76 J. H. Lee, *Sens. Actuators, B*, 2009, **140**, 319–336.

77 S. Virji, R. B. Kaner and B. H. Weiller, *J. Phys. Chem. B*, 2006, **110**, 22266–22270.

78 K. H. Hong, K. W. Oh and T. J. Kang, *J. Appl. Polym. Sci.*, 2004, **92**, 37–42.

79 N. V. Bhat, A. P. Gadre and V. A. Bambole, *J. Appl. Polym. Sci.*, 2001, **80**, 2511–2517.

80 O. S. Kwon, S. J. Park, H. Yoon and J. Jang, *Chem. Commun.*, 2012, **48**, 10526–10528.

81 X. X. Xing, L. L. Du, D. L. Feng, C. Wang, Y. Y. Tian, Z. X. Li, H. G. Liu and D. C. Yang, *Sens. Actuators, B*, 2022, **351**, 130944.

82 Y. Huang, E. Sutter, J. T. Sadowski, M. Cotlet, O. L. A. Monti, D. A. Racke, M. R. Neupane, D. Wickramaratne, R. K. Lake, B. A. Parkinson and P. Sutter, *ACS Nano*, 2014, **8**, 10743–10755.

83 C. Anichini, W. Czepa, D. Pakulski, A. Aliprandi, A. Ciesielski and P. Samori, *Chem. Soc. Rev.*, 2018, **47**, 4860–4908.

84 L. Yang, W. Xiao, J. Wang, X. Li and L. Wang, *RSC Adv.*, 2021, **11**, 37120–37130.

85 Y. J. Kwon, H. G. Na, S. Y. Kang, S.-W. Choi, S. S. Kim and H. W. Kim, *Sens. Actuators, B*, 2016, **227**, 157–168.

86 A. Vahl, O. Lupan, D. Santos-Carballal, V. Postica, S. Hansen, H. Cavers, N. Wolff, M.-I. Terasa, M. Hoppe, A. Cadi-Essadek, T. Dankwort, L. Kienle, N. H. de Leeuw, R. Adelung and F. Faupel, *J. Mater. Chem. A*, 2020, **8**, 16246–16264.

87 S. Kumar, S. Kumar, M. Sengar and P. Kumari, *RSC Adv.*, 2021, **11**, 13674–13699.

88 M. E. Franke, T. J. Koplin and U. Simon, *Small*, 2006, **2**, 36–50.

89 P. Jaroenapibal, P. Boonma, N. Saksilaporn, M. Horprathum, V. Amornkitbamrung and N. Triroj, *Sens. Actuators, B*, 2018, **255**, 1831–1840.

90 Z. Li, Y. Zhang, H. Zhang and J. Yi, *Sens. Actuators, B*, 2021, **344**, 130182.

91 X. Xing, Z. Li, X. Chen, L. Du, Y. Tian, D. Feng, C. Wang, G. Liu and D. Yang, *ACS Appl. Mater. Interfaces*, 2022, **14**, 17911–17919.

92 B. Xie, B. Ding, P. Mao, Y. Wang, Y. Liu, M. Chen, C. Zhou, H. M. Wen, S. Xia, M. Han, R. E. Palmer, G. Wang and J. Hu, *Small*, 2022, **18**, 2200634.

93 D. Wang, J. Yang, L. Bao, Y. Cheng, L. Tian, Q. Ma, J. Xu, H. J. Li and X. Wang, *J. Colloid Interface Sci.*, 2021, **597**, 29–38.

94 Z. Chen, J. Wang and Y. Wang, *Talanta*, 2021, **235**, 122745.

95 U. Latif and F. L. Dickert, *Sensors*, 2015, **15**, 30504–30524.

96 J. L. Johnson, A. Behnam, S. J. Pearton and A. Ural, *Adv. Mater.*, 2010, **22**, 4877–4880.

97 C. H. Park, W. T. Koo, Y. J. Lee, Y. H. Kim, J. Lee, J. S. Jang, H. Yun, I. D. Kim and B. J. Kim, *ACS Nano*, 2020, **14**, 9652–9661.

98 D. Zhang, D. Wang, W. Pan, M. Tang and H. Zhang, *Sens. Actuators, B*, 2022, **360**, 131634.

99 H. Jun, W. Tao, W. Yanjie, H. Da, H. Guili, H. Yutong, H. Nantao, S. Yanjie, Z. Zhihua, Z. Yafei and Y. Zhi, *Sens. Actuators, B*, 2018, **263**, 120–128.

100 C. S. Reddy, L. W. Zhang, Y. J. Qiu, Y. N. Chen, A. S. Reddy, P. S. Reddy and S. R. Dugasani, *J. Ind. Eng. Chem.*, 2018, **63**, 411–419.

101 S. Palimar, S. D. Kaushik, V. Siruguri, D. Swain, A. E. Viegas, C. Narayana and N. G. Sundaram, *Dalton Trans.*, 2016, **45**, 13547–13555.

102 Z. H. Wang, C. L. Hou, Q. M. De, F. B. Gu and D. M. Han, *ACS Sens.*, 2018, **3**, 468–475.

103 D. Degler, U. Weimar and N. Barsan, *ACS Sens.*, 2019, **4**, 2228–2249.

104 H. Chen, Y. Zhao, L. Shi, G. D. Li, L. Sun and X. Zou, *ACS Appl. Mater. Interfaces*, 2018, **10**, 29795–29804.

105 C. Zhao, H. Gong, G. Niu and F. Wang, *Sens. Actuators, B*, 2019, **299**, 126946.

106 M. Hjiri, F. Bahanan, M. S. Aida, L. El Mir and G. Neri, *J. Inorg. Organomet. Polym. Mater.*, 2020, **30**, 4063–4071.

107 S. Yang, G. Lei, H. Xu, Z. Lan, Z. Wang and H. Gu, *Nanomaterials*, 2021, **11**, 1026.

108 M. Kumaresan, M. Venkatachalam, M. Saroja and P. Gowthaman, *Inorg. Chem. Commun.*, 2021, **129**, 108663.

109 N. Jayababu, M. Poloju, J. Shruthi and M. V. R. Reddy, *RSC Adv.*, 2019, **9**, 13765–13775.

110 J. G. Ibanez, M. E. Rincon, S. Gutierrez-Granados, M. Chahma, O. A. Jaramillo-Quintero and B. A. Frontana-Uribe, *Chem. Rev.*, 2018, **118**, 4731–4816.

111 S. Li, A. Liu, Z. Yang, J. He, J. Wang, F. Liu, H. Lu, X. Yan, P. Sun, X. Liang, Y. Gao and G. Lu, *Sens. Actuators, B*, 2019, **299**, 126970.

112 H. Jin, T. P. Huynh and H. Haick, *Nano Lett.*, 2016, **16**, 4194–4202.

113 D. Zhang, C. Jiang, J. Liu and Y. Cao, *Sens. Actuators, B*, 2017, **247**, 875–882.

114 M. Ikram, H. Lv, Z. Liu, K. Shi and Y. Gao, *J. Mater. Chem. A*, 2021, **9**, 14722–14730.

115 W. Wang, X. H. Xiong, N. X. Zhu, Z. Zeng, Z. W. Wei, M. Pan, D. Fenske, J. J. Jiang and C. Y. Su, *Angew. Chem., Int. Ed.*, 2022, **61**, e202201766.

116 D. F. Lv, P. J. Zhou, J. H. Xu, S. Tu, F. Xu, J. Yan, H. X. Xi, W. B. Yuan, Q. Fu, X. Chen and Q. B. Xia, *Chem. Eng. J.*, 2022, **431**, 133208.

117 C. S. Diercks, Y. Z. Liu, K. E. Cordova and O. M. Yaghi, *Nat. Mater.*, 2018, **17**, 301–307.

118 L. H. Shi, N. Li, D. M. Wang, M. K. Fan, S. L. Zhang and Z. J. Gong, *TrAC, Trends Anal. Chem.*, 2021, **134**, 116131.

119 J. Xue, Q. Sun, Q. Li and J. Qian, *CrystEngComm*, 2022, **24**, 3649–3655.

120 J. Ding, L. Zhong, X. Wang, L. Chai, Y. Wang, M. Jiang, T.-T. Li, Y. Hu, J. Qian and S. Huang, *Sens. Actuators, B*, 2020, **306**, 127551.

121 R. Zhang, L. Lu, Y. Chang and M. Liu, *J. Hazard. Mater.*, 2022, **429**, 128321.

122 X. L. Zhang, Z. Y. Zhai, J. N. Wang, X. K. Hao, Y. X. Sun, S. Y. Yu, X. Q. Lin, Y. Qin and C. J. Li, *Chemnanomat*, 2021, **7**, 1117–1124.

123 W. T. Koo, S. Qiao, A. F. Ogata, G. Jha, J. S. Jang, V. T. Chen, I. D. Kim and R. M. Penner, *ACS Nano*, 2017, **11**, 9276–9285.

124 T. T. Tung, M. T. Tran, J.-F. Feller, M. Castro, T. Van Ngo, K. Hassan, M. J. Nine and D. Losic, *Carbon*, 2020, **159**, 333–344.

125 D. Zhang, Z. Yang, S. Yu, Q. Mi and Q. Pan, *Coord. Chem. Rev.*, 2020, **413**, 213272.

126 Y. Ding, X. Guo, B. Du, X. Hu, X. Yang, Y. He, Y. Zhou and Z. Zang, *J. Mater. Chem. C*, 2021, **9**, 4838–4846.

127 X. Chang, X. Li, X. Qiao, K. Li, Y. Xiong, X. Li, T. Guo, L. Zhu and Q. Xue, *Sens. Actuators, B*, 2020, **304**, 127430.

128 Y. Xu, J. Xie, Y. Zhang, F. Tian, C. Yang, W. Zheng, X. Liu, J. Zhang and N. Pinna, *J. Hazard. Mater.*, 2021, **411**, 125120.

129 M. Han, S. Jung, Y. Lee, D. Jung and S. H. Kong, *Micromachines*, 2021, **12**, 1053.

130 R. K. Sonker, S. R. Sabhajeet and B. C. Yadav, *J. Mater. Sci.: Mater. Electron.*, 2016, **27**, 11726–11732.

131 M. Chen, P. Mao, Y. Qin, J. Wang, B. Xie, X. Wang, D. Han, G. H. Wang, F. Song, M. Han, J. M. Liu and G. Wang, *ACS Appl. Mater. Interfaces*, 2017, **9**, 27193–27201.

132 D. Zhang, Y. e. Sun, C. Jiang, Y. Yao, D. Wang and Y. Zhang, *Sens. Actuators, B*, 2017, **253**, 1120–1128.

133 J. Liu, L. Zhang, B. Cheng, J. Fan and J. Yu, *J. Hazard. Mater.*, 2021, **413**, 125352.

134 D. Wang, Z. Li, J. Zhou, H. Fang, X. He, P. Jena, J. B. Zeng and W. N. Wang, *Nano-Micro Lett.*, 2018, **10**, 4.

135 Z. Zhu, X. Xing, D. Feng, Z. Li, Y. Tian and D. Yang, *Nanoscale*, 2021, **13**, 12669–12675.

136 J. Li, Q. Ding, X. Mo, Z. Zou, P. Cheng, Y. Li, K. Sun, Y. Fu, Y. Wang and D. He, *RSC Adv.*, 2021, **11**, 39130–39141.

137 J. Y. Zhou, J. L. Bai, H. Zhao, Z. Y. Yang, X. Y. Gu, B. Y. Huang, C. H. Zhao, L. Cairang, G. Z. Sun, Z. X. Zhang, X. J. Pan and E. Q. Xie, *Sens. Actuators, B*, 2018, **265**, 273–284.

138 A. Hermawan, Y. Asakura, M. Inada and S. Yin, *J. Mater. Sci. Technol.*, 2020, **51**, 119–129.

139 S. U. Din, M. U. Haq, R. Khatoon, X. Chen, L. Li, M. Zhang and L. Zhu, *RSC Adv.*, 2020, **10**, 21940–21953.

140 H. Liu, W. Zhang, H. Yu, L. Gao, Z. Song, S. Xu, M. Li, Y. Wang, H. Song and J. Tang, *ACS Appl. Mater. Interfaces*, 2016, **8**, 840–846.

141 H. Tian, H. Fan, M. Li and L. Ma, *ACS Sens.*, 2015, **1**, 243–250.

142 T. Zhou, Y. Sang, X. Wang, C. Wu, D. Zeng and C. Xie, *Sens. Actuators, B*, 2018, **258**, 1099–1106.

143 D. M. ME, N. G. Sundaram and S. B. Kalidindi, *Chemistry*, 2018, **24**, 9220–9223.

144 A. Abun, B.-R. Huang, A. Saravanan, D. Kathiravan and P.-D. Hong, *ACS Appl. Nano Mater.*, 2020, **3**, 12139–12147.

145 M. A. Farea, H. Y. Mohammed, P. W. sayyad, N. N. Ingle, T. Al-Gahouari, M. M. Mahadik, G. A. Bodkhe, S. M. Shirsat and M. D. Shirsat, *Appl. Phys. A*, 2021, **127**, 681.